PROCESS MODELING FOR PROJECTION BASED STEREO LITHOGRAPHY

A THESIS SUBMITTED TO
THE GRADUATE SCHOOL OF ENGINEERING AND SCIENCE
OF BILKENT UNIVERSITY
IN PARTIAL FULFILLMENT OF THE REQUIREMENTS FOR
THE DEGREE OF
MASTER OF SCIENCE
IN
MECHANICAL ENGINEERING

By
Zulfiqar Ali
August, 2015

Process Modeling for Projection Based Stereo Lithography
By Zulfiqar Ali
August, 2015

We certify that we have read this thesis and that in our opinion it is fully adequate, in scope and in quality, as a thesis for the degree of Master of Science.

Assist. Prof. Yiğit Karpat (Advisor)

Assist. Prof. Melih Çakmakcı

Assist. Prof. Yiğit Taşçıoğlu

Approved for the Graduate School of Engineering and Science:

Prof. Levent Onural
Director of the Graduate School

ABSTRACT

PROCESS MODELING FOR PROJECTION BASED STEREO LITHOGRAPHY

Zulfiqar Ali
M.S. in Mechanical Engineering
Advisor: Assist. Prof. Yiğit Karpat
August, 2015

Stereo lithography is a widely used additive manufacturing process, where a three dimensional object is fabricated directly from a solid computer model. This thesis develops a projection type SLA (PSLA) test bed using a digital micro mirror device. The goal is to improve the dimensional accuracy and surface quality of the polymer parts through detailed process modeling and gain predictive ability about the duration of the printing process. For that purpose; (i) process parameters of the PSLA system have been analyzed, (ii) material properties of different polymers have been identified through experimental techniques, and a curing process model has been established, and (iii) some case studies have been conducted. The information deduced from the system is used to set the continuous movement speed of the vertical axis to obtain "layerless printing" of parts where the surface quality is significantly improved compared to conventional layer-by-layer printing. The results show that the process planning approach used in this thesis can produce highly accurate parts. Experiments on more challenging part designs such as high aspect ratio and micro scale parts have also been conducted, and limits of the three dimensional printing system have been determined.

Keywords: Additive manufacturing, stereo lithography, projection Stereo lithography, Digital micromirror device (DMD).

ÖZET

PROJEKSIYON TEMELLI STEREO LITHOGRAFI PROSES MODELLENMESI

Zulfiqar Ali
Makine Mühendisliği, Yüksek Lisans
Tez Danışmanı: Assist. Prof. Yiğit Karpat
Ağustos, 2015

Stereo litografi katmanlı üretim alanında sıkça kullanılan bir üretim yötemi olup üç boyutlu paraçaların katı bilgisayar modelinden doğrudan üretilmesine olanak sağlar. Bu tezde dijital mikro ayna cihazı kullanan projeksiyon temelli bir stereo litografi sistemi geliştirilmiştir. Amaç üretilen paraçaların boyutsal ve yüzey kalitelerinin iyileştirilmesi ve üretim süresinin tahminini proses modelleme tekniklerinin kullanılarak yapılmasıdır. Bu amaca yönelik olarak; (i) proses parametreleri araştırımış, (ii) değişik polimerlerin malzeme özellikleri deneysel yöntemler ile incelenmiş ve bir kürleme modeli elde edilmiş, (iii) bazı örnek çalişmalar üzerinde sistem test edilmiştir. Kürleme modelı üzerinden elde edilen bilgi ile düşey eksen harekt hızı belirlenmiş ve bu devamlı hareket sonucunda katmansız üretim gerçekleştirilmiş ve üstün yüzey kalitesine sahip paraçlar üretilmiştir. Sonuçlar proses planlama yaklaşımı ile yüksek hassasiyette paraçaların bu metod ile üretilebileceğini göstermektedir. Üretilmesi daha zor olan yüksek boy ve kalınlık oranına sahip ve mikro ölçek parça gibi tasarımlar üzerinde denemeler yapılmış ve mevcut üç boyut baskılama sisteminin limiteri belirlenmiştir.

Anahtar sözcükler: Katmanlı üretim, Stereo lithografi, Sayısal micro ayna aygıtı.

Acknowledgement

I take this opportunity to express my sincere appreciation to my advisor Dr.Yiğit Karpat for his understanding, support, patience, inspiration and confidence in my abilities. He was always with me during the tough time in Bilkent University especially when I was under huge amount of stress of transferring from industrial engineering department to mechanical engineering department. His generous offer to accept me as his MS student in Bilkent University helped me to fulfill my wish of studying abroad. His rich experiences and insights have navigated me to conduct quality research. I will be grateful to his nice personality and excellent guidance forever. I would like to thank Dr.Melih Çakmakcı and Dr. Yiğit Taşçıoğlu for reading and reviewing my thesis.

I was fortunate to have colleague like Erkan Bugra Treyen, my super-team player, without his diligent contributions, the work I am going to present in this thesis is impossible. I am grateful to his tremendous efforts in improving the setup of DLP based Projection stereolithography via doing numerous experiments as well as in helping me with the documentation and experimental validations. Also, I want to thank Dr.Atilla Aydinli from the Physics department of Bilkent University for allowing me to use his equipment for irradiance measurements of DLP Projector.

I would like to thank my lab mate Mr.Samad Nadimi Bavil Oliaei whose rich experience in manufacturing help me a lot for thinking outside of the box. In addition, I would like to thank Stefan Ristevski, A.Y Tiftikci, Abdullah Waseem, Serhat Kerimoglu, Neginsadat Musavi, Arsalan Nikdoost, Reza Rasooli, Mustafa Kılıc and other graduate students of Mechanical engineering department in Bilkent University for their best wishes and support through out this journey. Also, I would like to thank my dormitory friends with whom I find this place like home. I especially cherish the friendship of Mehrab Ramzan, Tufail Ahmed, Asad Ali, Abdul Ali Kakar, Mubin Memon, Shahid Ali Leghari, Muhammad Maiz Ghouri, Ebrima Tunkara, Emir, Ateeq Ur Rehman, Saghir Abbas, Sabeeh Iqbal, Furqan Ali and many more. I have a great time with all of you.

I would like to thank my parents and my whole family for supporting me

through out my life in difficult situation. I especially cherish the love of my elder brothers Javed Ali and Farmaish Ali. I have no words to express the profound love and respect that I have for them, not just as my brothers, but also as mentor.

Finally, I would also like to thank Tubitak (The Scientific and Technological Research Council of Turkey) for the financial supports to the project no 113M172 which help me to conduct a quality research without worrying the financial side of my life.

Contents

List of Figures

List of Tables

Chapter 1

Introduction

1.1 Additive Manufacturing

Additive Manufacturing (AM) is the new technology in manufacturing field that is used to produce three-dimensional objects. The promise of this technology is that, at first a model is created using a three-dimensional Computer Aided Design (3D CAD) system that could be manufactured directly without the need of process planning. Although it is not in reality as simple as it first sounds, AM technology significantly simplifies the process of producing complex 3D parts directly from CAD data. Other manufacturing processes require a careful and detailed analysis of the part geometry to determine things like the order in which different features can be fabricated, what tools and processes must be used, and what additional fixtures may be required to complete the part. However, AM needs only some basic dimensional details of the part and a small amount of understanding about the parameters of AM machine that how the AM machine works [1].

The key to how AM works is that parts are made by adding material in layers; each layer is a thin cross-section of the part derived from the original CAD data. Obviously in the physical world, each layer must have a finite thickness to it and so the resulting part will be an approximation of the original data, as illustrated by Fig 1.1. The fabricated part will be closer to the original design if the layer

thickness of each layer is thinner. All commercialized AM machines to date use a layer-based approach; and the major ways that they differ are in the materials that can be used, how the layers are created, and how the layers are bonded to each other. Such differences will determine factors like the accuracy, material properties and mechanical properties of the final part. They will also determine factors like how quickly the part can be made, how much post processing is required, the size of the AM machine used, and the overall cost of the machine and process [1, 2].

Figure 1.1: CAD image of a teacup with further images showing the effects of building using different layer thicknesses [1].

1.1.1 The Generic Additive Manufacturing Process

AM involves a number of steps that move from the virtual CAD description to the physical resultant part as shown in Fig 1.2.

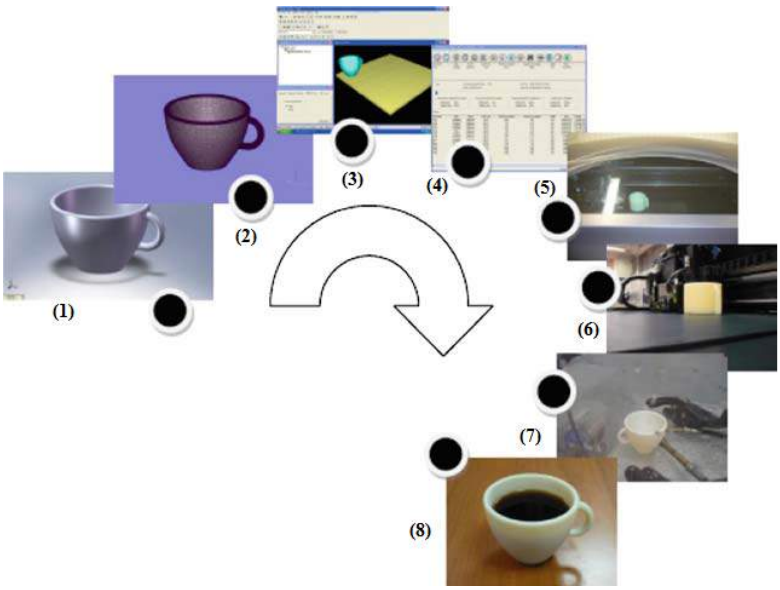

Figure 1.2: Generic process of CAD to part, showing all 8 stages [1].

Regardless of the AM machine, the process can be divided into eight key steps as shown 1.2.

1. CAD file of the desired part
2. Convert it to STL format.
3. Transfer the file to machine
4. Machine setup
5. Build the model
6. Part removal and Cleanup
7. Post-Processing of the Part
8. Application of the printed part

1.1.2 Additive Manufacturing Methodologies

Additive Manufacturing technology has been used for different applications. For instance, it has been successfully utilized in the process of entitled contour crafting, automatized construction of buildings. This AM process is developed by Prof. Behrokh Khoshnevis from the University of Southern California, USA. The basic idea of contour crafting is that a house can be made in a additive layer manner using concrete as a layer. With this method it may be possible to build a house in one day or a whole block of houses rapidly and cost efficiently [3,4]. Even it is used to print food using a 3D printer, which they called a "food printer". For instance, researchers at the University of Exeter have developed a 3D printer that uses chocolate instead of ink or plastic as a basic layer material [5].

There is a wide range of different AM process, which differs mostly in the material utilized. The discriminating feature of AM is that these methods create the whole structures in one fabrication step while other techniques use several steps to made a product [6, 7]. Materials range from plastic to metals and sand. For example, plastics are utilized for stereolithography (SLA) and metal powders for selective laser sintering (SLS). The material characterizes the layer creation technique and the mechanical properties of the final product.

Researchers around the world has done tremendous work on studying the resolution and features of additive manufacturer methods. Summary of the resolution and the minimum feature size for of different additive manufacturing methods has been shown in Table 1.1 [7].

Process Parameter	Stereo-lithography (SLA)	Selective Laser Sintering (SLS)	Micro Laser Sintering (MLS)	Fused Deposition Modeling (FDM)	Polyjet
Layer thickness (μm)	50-100 (HR) 120-150 (SR)	100	2-4	180-250	16 (HR) 30(LR)
Min feature size (μm)	250-380 (HR) 630-890 (SR)	750-1000	32	630	600 (HR) 1100(LR)
Material Selection	Various ABS like rigid and clear poly carbonate: semi-flexible polyethylene.	Nylons (including glass-filled, flame retardant durable)	Moly-bdenum SS316L Chrome alloy Aluminum, Nickel alloy Titanium Nylon	ABS, Poly carbonate ,Polyphenyl sulfone	Rigid elastomeric, translucent , opaque ,ABS, poly propylene.
Max model (mm)	600*700*500	300*300*400	55*55*30	600*700*500	500*400*200
Comments	ABS can ultrasonically welded	Heat and chemically resistant materials	Bio compatible materials conductive materials	Available in various colours, soluble support materials	Allows custom creation of materials from the library of materials, Meltable support

Table 1.1: Process Capabilities of Different Additive Manufacturing Methods [7].

where:

- HR=High Resolution
- SR=Standard Resolution
- LR=Low Resolution

1.2 Stereolithography

Stereolithography (SLA) also known as optical fabrication, photo-solidification, solid free-form fabrication, solid imaging or resin printing. It is an additive manufacturing technology that is used for producing prototypes, patterns or production parts up to one layer at a time by curing a photo-reactive resin with a UV power source. It is often considered the pioneer of the rapid prototyping industry with first commercial system introduced in 1988 by 3D System [8]. The system consists of an Ultra-Violet Laser, a vat of photo-curable liquid resin and a controlling system as shown in Fig 1.3.

The model is manufactured by consecutively polymerizing layers made by the software in the SLA tool utilizing a CAD file as its input. At first, a platform is loaded with the photo polymer to the thickness of the first layer (50-150 μm) and a laser beam scans the surface to polymerize the layer as shown in Fig 1.3.

The platform is then brought down by a layer thickness, the polymer is apportioned and the laser beam polymerizes it again and the process is repeated until the whole model is manufactured [8, 9]. Once the model is complete, the platform rises out of the vat and the excess resin is drained. The model is then removed from the platform, washed of excess resin and then placed in a UV oven for final curing to keep any undesirable synthetic responses that normally lead dimensional inaccuracy, fractures and distortion. Such layer-by-layer procedure brings about surface roughness that may need to be uprooted in a different steps.

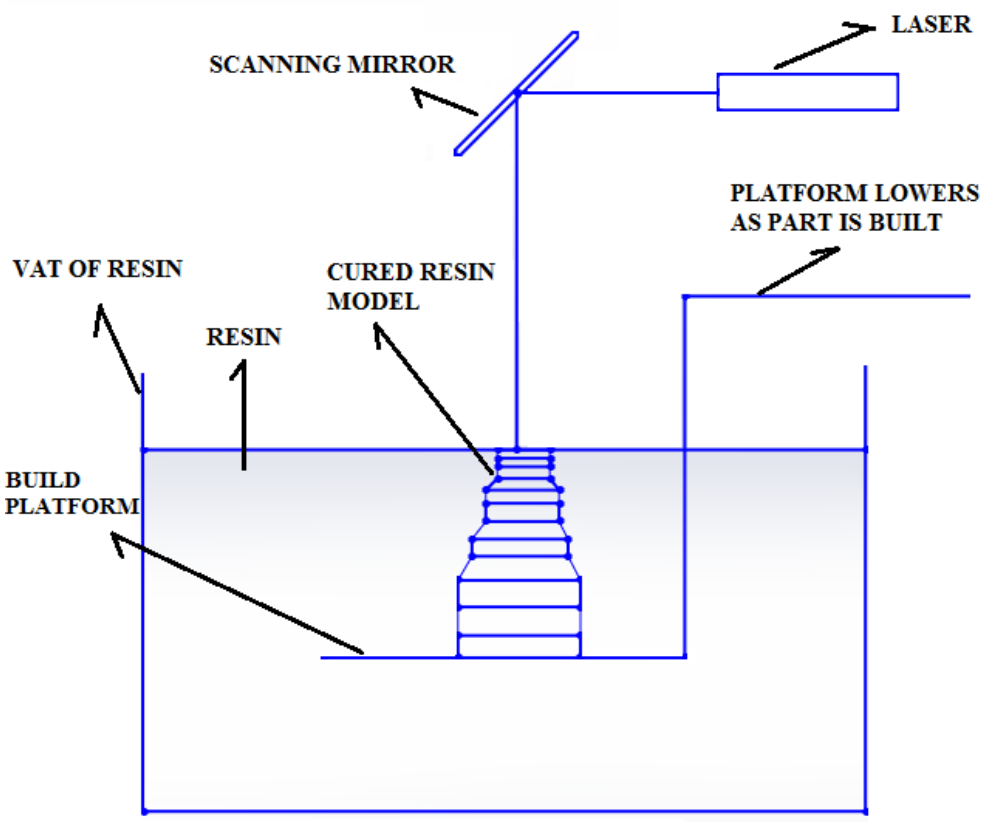

Figure 1.3: Working Mechanism of Stereolithography

1.2.1 Sterelithography Materials

Epoxy based materials have been used in stereolithography resins. These material offer strong, durable and accurate models and ideal for fit, form and function testing purposes. Usually SLA materials have a low heat tolerance with typical heat deflection temperatures around 110-120F [8]. The mechanical properties of different SLA materials has been listed in Table 1.2.

1.2.2 Resolution

There are two types of resolution that plays a vital role in the accuracy of the produced parts. Vertical resolution (VR) and Lateral resolution (LR). Lateral resolution mainly depends upon the minimum size of the projected image on the platform and light intensity from the light source which effect the quality of the image that is projected on the platform. Vertical resolution depends on the layer thickness and the vertical-axis movements.

1.2.3 Microstereolithography

Microstereolithography (μSLA) as its name suggests is used to address the requirement for finer resolution in 3D printing utilizing photosensitive materials. While technically it is very much alike to stereo lithography in the utilization of photo polymerization by a light source. In microstereolithography, the image could be made through the utilization of a finely centered stationary laser beam with the platform loaded with photo-resin moving in a precise pattern, structuring the part with high resolution yet at the cost of noteworthy manufacturing times. The resolution is a few micrometers both in the lateral and vertical direction. Two-photon polymerization technique can achieve resolution of sub-50 nm [8].

Originally μSLA was developed to produce high precision 3D MEMS (micro electro-mechanical systems) parts [10, 11]. Also μSLA can be used to produce useful components for microfluidic, micro robotic and biomedical applications. For instance, artificial blood vessels could be made by combining 3D printing

Mechanical Properties	**Test Method**	**Units**	**Rigid Resin (Somos 10120)**	**Water Clear Resin (Somos 10120)**	**Durable (Somos 9100)**	**Durable (SL 7540**	**Semi Flexible (Somos 8100)**
Tensile Strength	ASTM D638	psi	6237	6237	4700	5500	3800
Tensile Modulus	ASTM D638	psi	318000	318000	212000	223000	73500
Tensile Elongation at break	ASTM D638	psi	18%	18%	25%	11-22%	22%
Flexural Modulus	ASTM D790	psi	11000	11000	6700	7000	3700
Hardness	DIN 53505 /2240	Shore D	83	83	82	79	81
Izod Impact Notched	ASTM D256	(ft-1b) /in	0.57	0.57	1	0.72	1.1
Heat Deflection Temp	ASTM D648 D648	deg F	136	136	142	135	130

Table 1.2: Commercial Stereolithography Material Properties [8].

technology and two-photon polymerization [12], which may also be possible using high performance μSLA equipment.

SLA is known for high fabrication speed, part precision and surface finish. However, SLA machines are costly, because of the utilization of a laser and a scanner framework, contrasted with various 3D printers [1]. By using projection technique in SLA, one may significantly reduce the equipment costs. The laser and scanner system are replaced by a dynamic mask generator i.e. liquid crystal display (LCD) or digital micro mirror device (DMD) and a lamp. Thus, the resin will be selectively cured according to the pattern on the dynamic mask generator. An entire layer is manufactured at once, rather than vector by vector as in scanning SLA machine. The projection stereolithography (PSLA) technique lowers the machine cost and is more robust, since only one translation is required [8]. The cost of AM equipment frequently connects with the fabrication accuracy and the material utilized. Economical do-it-yourself (DIY) 3D printer setup may cost less of what 1000 €, while metal laser sintering machines may cost in excess of 500,000 € [2, 8].

1.3 Motivation and Objective

The thesis work presented here is developed as part of a TUBITAK project titled 'Development of an Multipurpose Micro Manufacturing System using Modular and Iterative Learning Control Algorithms (113M172)' in which different manufacturing methods including micro laser machining, rapid micro prototyping and micro milling is studied for a flexible micro-machining device. The goal of this study is to construct a DLP based Projection stereo lithography 3D printer that is capable of producing 3D structures with few micrometers accuracy. With only a few PSLA systems developed and studied so far with an accuracy in the same range of commercial systems, the research in this field is inchoate and experimental in nature.

Basically this setup consist of DLP projector,various optical components, resin vat, a linear translation stage with a platform that is controlled by a computer. These components have been assembled together to make a 3D printing machine.

The working mechanism of the setup is that the CAD model is sliced into horizontal cross section images. These black and white images will be projected one by one onto the resin. The computer program will handle the changing of images as well as sending movement commands to the linear translation stage that moves the platform upon which the part is built. It is important that the image projection and platform movement are synchronized to avoid part manufacturing failures. Before the actual manufacturing process, the computer program should accept several input parameters, such as layer thickness, platform movement speed, exposure time and image projection size. Uniform exposure is important to acquire precise control of the curing process.

These parameters make the equipment versatile and suitable for a wide range of different tasks such as layerless fabrication of parts. It is possible to produce both layer by layer production or layerless production of parts by changing the parameters of the system. In order to employ the PSLA technology for fabrication, it is necessary to model its part building process and formulate a process planning method to cure dimensionally accurate parts. A Image formation and cure model has been established and verify via experiments for curing dimensionally accurate parts in the lateral direction. The process of curing a single layer using this system is analytically modeled as "cure model".

Chapter 2

Literature Review

In this chapter there will be brief literature review of different stereo lithography setups that has been build in different places across the globe.

2.1 PμSLA setup of Sun et al.

A high-resolution projection micro-stereolithography (PμSLA) process has been developed by Sun et al in University of California Los Angeles by using the Digital Micromirror Device as a dynamic mask [13]. Sun et al. call the system a projection microstereo-lithography apparatus (PμSLA) as shown in Fig 2.1. The uniformity of the light being emitted from the mercury lamp was considered critical to maintain the process reliability. This homogeniser maintained illumination intensity within a $\pm$ 5% variation. The platform mechanism was motorised and coordinated by computer control. The layer translation had an effective precision of 0.1μm [13]. This setup was an integration of many sub-systems, which function in cooperation to provide correct exposure and layer thickness control. The five main components are identified as: the Digital Micro mirror device, a projection lens, a UV light source, a motor base translation system for platform movement, and a vat containing UV curable resin.

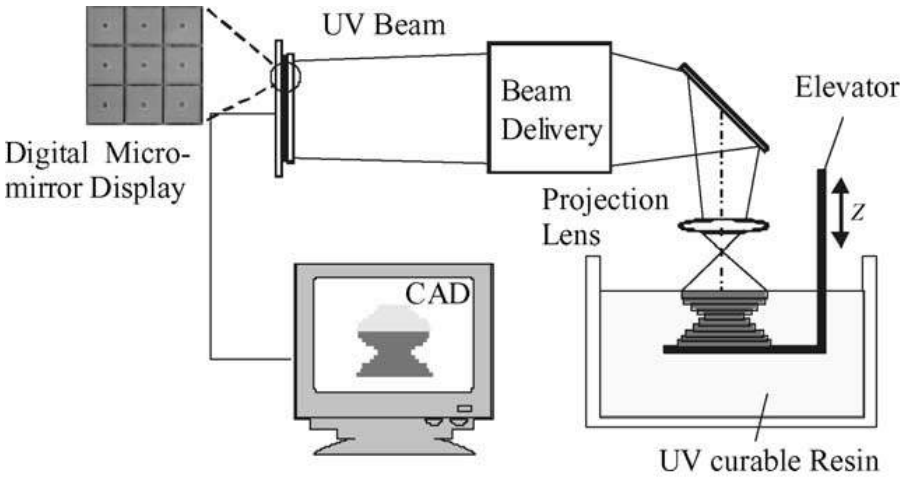

Figure 2.1: Schematic diagram of projection micro-stereolithography (PμSLA) apparatus [13].

2.1.1 Process Model

In the process modeling of (PμSLA), the spread of radiation flux has been described by the point spread function(PSF). The Gaussian distribution was used as the first order approximation of PSF to describe the flux-density contribution of light spot from the image plane. The flux density contribution E(x) and the

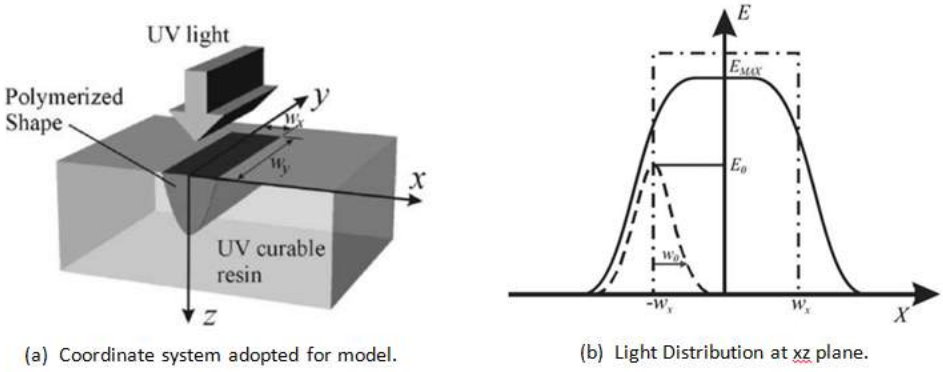

Figure 2.2: Process modeling of (PμSLA) apparatus [13].

irradiation at any point in the resin E(x,y,z) was defined in Equation 2.1 and Equation 2.2 where E_0 and w_0 was the peak intensity and Gaussian radius.

Also UV light absorption was described by the Beer-Lambert law defined in Equation 2.3.

$$E(x) = E_0 exp(-x^2/w_0^2) \tag{2.1}$$

$$E(x, y, z) = E(x, y, 0) exp(-z/D_p) \tag{2.2}$$

$$C_d = D_p ln(E_(max)/E_c) \tag{2.3}$$

In Equation 2.2 the D_p is the light penetration depth of the resin which was found from "working curve equation" of the resin as shown in Fig 2.3. By introducing 0.3% UV doping has decreased the curing depth of the resin from 163 to 45 μm. The introduction of 0.3% UV doping means that the concentration of chemical ingredient in the resin which absorb UV light has increase 0.3% that slow down the polymerization process. The cure depth of the resin will decrease if the concentration of the UV absorber will increase as shown in Fig 2.3.

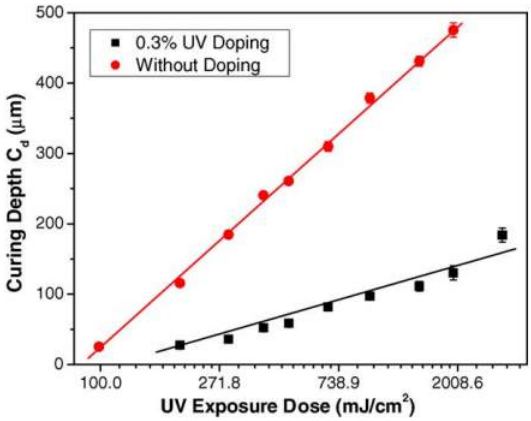

Figure 2.3: Working curve of the resin with different doping levels of UV light [13].

2.1.1.1 Sample Production

Different 3D micro structures had been fabricated via this system which are shown in Fig 2.4. A layer base curing approach was used for these microstructures e.g. a micro-matrix was fabricated by 110 layers with the layer thickness of 5 μm as shown in Fig 2.4(a). By adding more sliced layers, a microstructure with even higher aspect ratio can also be built.

The micro rod array consists of an array of rods with an extremely high aspect ratio as shown in Fig 2.4b. The rods shown in Fig 2.4(b) present uniform dimensions with 30μm in diameter, and 1000μm in height, which correspond to the aspect ratio of 33:1. The PμSL was not only advanced in constructing high aspect ratio structures, but it was also capable for producing sophisticated 3D micro-structures. The PμSL accomplishes this by fabricating an array of 3×3 micro-coil into 108 layers, with each layer having a thickness of 5 μm. The diameter of the coil and the wire were $150\mu m$ and 15μm respectively as shown in Fig 2.4(c). The minimum feature size was demonstrated through the fabrication of suspended beams with a diameter of 0.6μm as shown in Fig 2.4 (d).

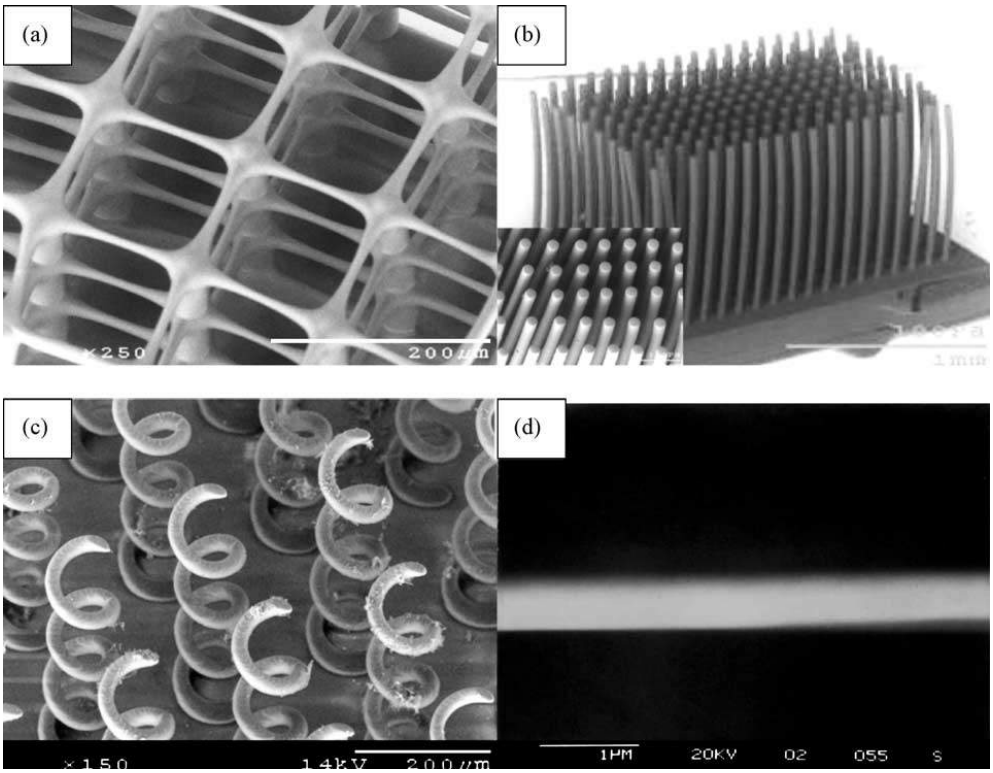

Figure 2.4: 3D microstructures fabricated by PμSL process: (a) micro matrix with suspended beam diameter of 5μm; (b) high aspect-ratio micro rod array consists of 21×11 rods with the overall size of $2mm \times 1mm$. The rod diameter and height is of 30 μm and 1 mm, respectively; (c) micro coil array with the coil diameter of 100 μm and the wire diameter of 25 μm (d) suspended ultra fine line with the diameter of 0.6 μm [13].

2.2 Hadiposespito PμSLA Setup

Hadiposespito and Li designed a Micro-SLA setup in University of Wisconsin-Madison using DMD to build meso/micro structures [14, 15]. Their research was aimed at improving the layer thickness and process efficiency of existing PμSLA. Fig 2.5 shows the layout of their system. A 100W mercury lamp was used as the UV light source. The resin was optimised to cure at 355nm, without filtering the light.

The light was put through a fibre optic light guide and collimated. A total internal reflection (TIR) prism was used to direct the light onto the DMD. The resolution of the DMD was 1024×768(XGA) and the pixel size of each micro-mirror was $13.7\mu m \times 13.7\mu m$. The P$\mu$SLA used a silica window, known as a "dip-in"window, coated with Teflon film to prevent cured resin from sticking to the window.

2.2.1 Resin Characterization

Experiments were performed on the resin to determine the relationship between curing depth and exposure time. To find this relationship, Hadiposespito and Li rapid prototyped a thick support with a circular portion left uncured. The final layer closed the circle and was cured for a predetermined exposure time. Thus the curing depth was obtained from the measured thickness of the circle. The experimental procedure is shown in Fig 2.6. They have found that the curing depth was directly proportional to the exposure time for the exposure time range of 20 seconds that they tested.

Also they have defined the vertical and lateral resolution of an PμSLA setup. The vertical resolution was the minimum layer thickness that could be realized in the z-axis and was limited by the mechanism of the z-stage which is 5μm. Lateral resolution was the resolution in the x-y plane and indicated the smallest feature possible in this plane which is 20μm.

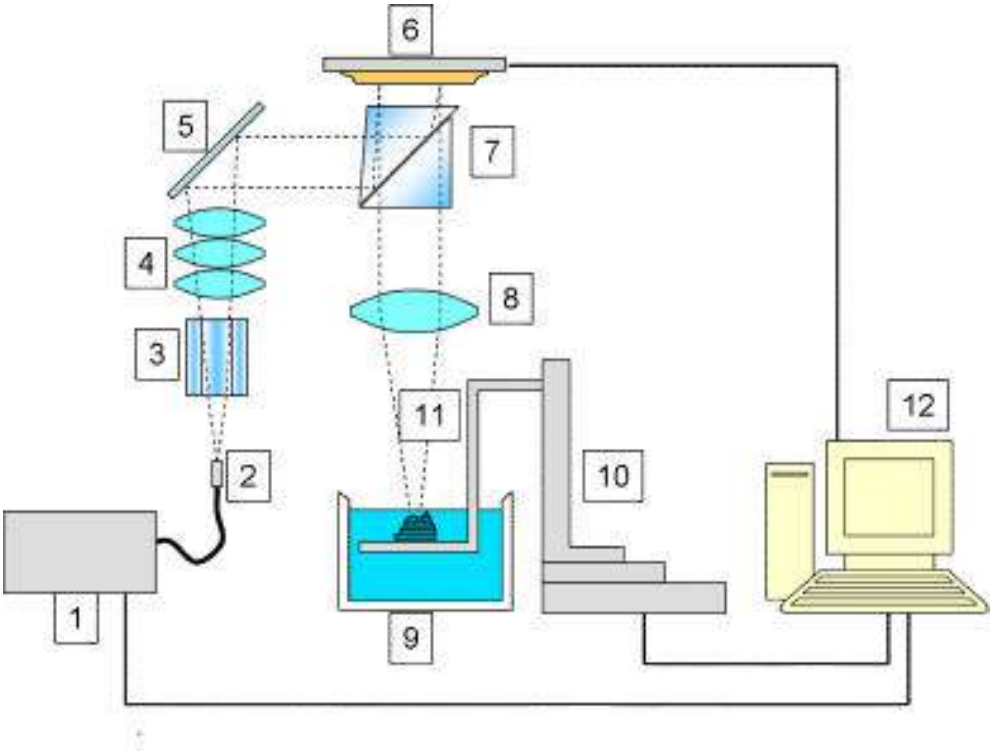

Figure 2.5: Diagram of the microstereolithography apparatus: (1) UV light source; (2) light guide; (3) light pipe; (4) condenser lens system; (5) fold mirror; (6) DMD; (7) TIR prism pair; (8) focusing lens system; (9) photopolymer bath; (10) x-y-z movable stage; (11) building platform; and (12) computer controller [14, 15].

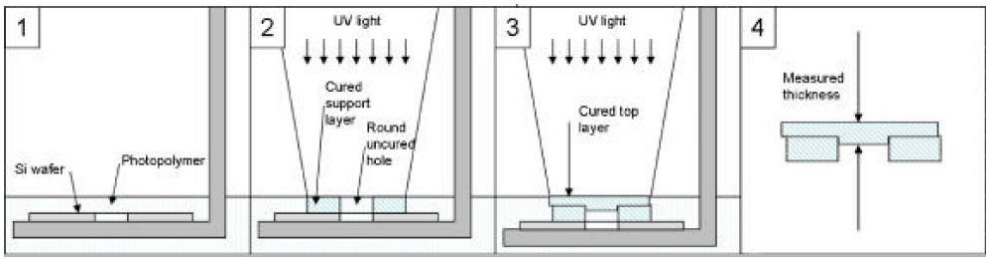

Figure 2.6: Experimental Procedure to find curing depth [14, 15].

2.3 Limaye PμSLA Setup

Limaye designed a PμSLA setp in Georgia Institute of Technology that used a DMD with a pixel size of $13.7\mu m \times 13.7\mu m$ [15,16]. The maximum part size made from this system is the area of $2mm \times 2mm$ ($450 \times 450 pixels$). A 50W mercury lamp was used as a light source and the light was emitted through a fiber optic light guide before the optical conditioning as shown in Fig 2.7.

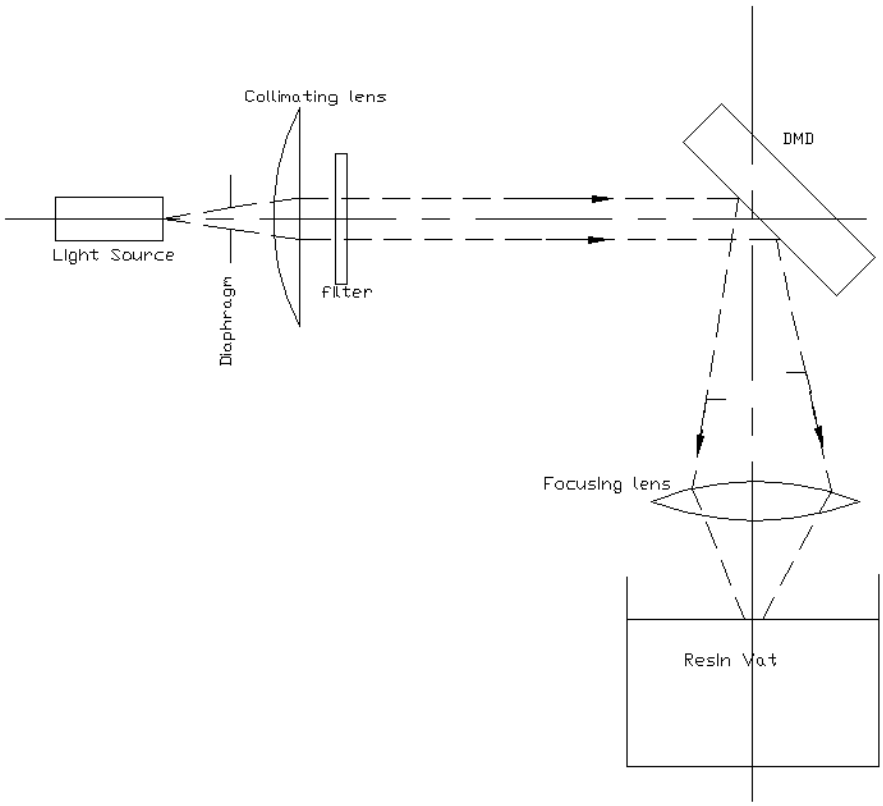

Figure 2.7: Working Mechanism of Limaye setup [16].

2.3.1 Layer Cure Model

The main contribution of his work was the analytically modeling of the process of curing a single layer as Layer cure model. The Layer cure model is formulated in two steps. First, the irradiance received by the resin surface is modeled as

a function of the system parameters (Irradiance model) and other is formulated using the resin parameters which is called cure model.

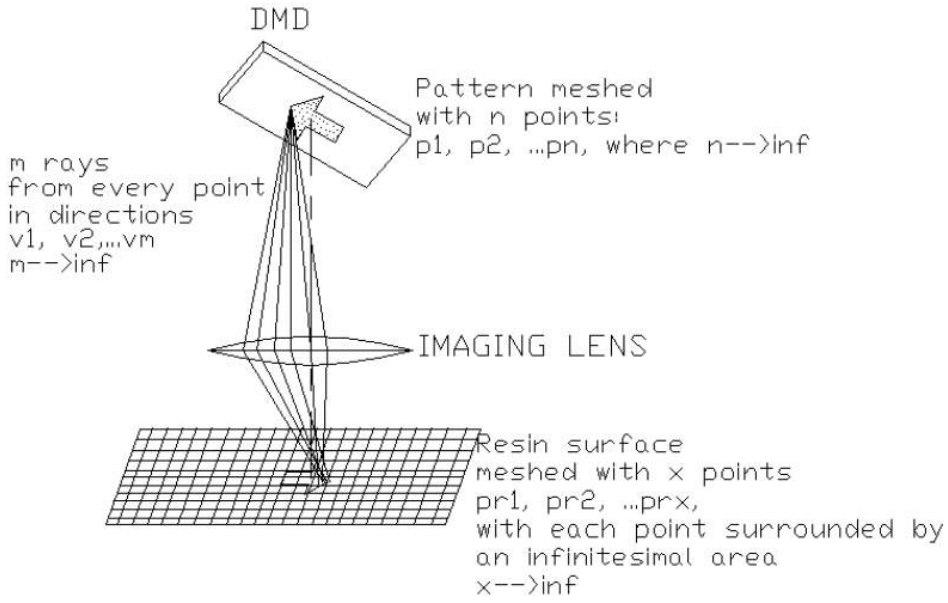

Figure 2.8: Nomenclature used for modeling the process [16].

The irradiance model of the system is shown in Equation 2.4 and cure model is in Equation 2.5.

$$H(pr_i) = (H_{av}x/\sum_{j=1}^{n} w_j m)\sum_{j=1}^{n}\sum_{k=1}^{m}\delta(p_j, v_k, pr_i, o, i, \alpha, d, d^{'}, \phi) \tag{2.4}$$

Then, the resin used in the system is characterized to experimentally determine its working curve and model as a layer cure model. The cure depth at any point pr_i

$$C_d(pr_i) = D_p ln(H(pr_i)TOE/E_c) \tag{2.5}$$

A function L(pr_i) was introduce to see that cured depth at a particular point is great than or equal to layer thickness(LT). If $C_d(pr_i) \geq LT$ than L(pr_i)=1 else L(pr_i)=0.
Where;

- H(pr_i) is irradiation received at point pr_i on the resin surface.
- H_{av} is the average irradiance received by the resin surface.
- w_j is the weight given to the ray, calculated as $w_j = 1 - 0.000\,86\mathrm{p} - 0.000\,83p^2$ where p is the distance of the point on the pattern from which the ray is emanating from the center of the beam incident on the DMD.
- $\delta(p_j, v_k, pr_i, o, i, \alpha, d, d^{'}, \phi)$ is a ray tracing function that operates on the imaging system parameters to determine whether the ray starting from pattern point p_j in the direction of vector v_k will intersect the point p_{ri} on the resin surface or not.
- $C_d(pr_i)$ is the cure depth at the point p_{ri} on the resin surface.
- $H(pr_i)$ is the irradiance received by the point p_{ri} on the resin surface.
- TOE is the time for which the pattern is imaged onto the resin surface
- D_p is the depth of penetration of the resin.
- E_c is the critical exposure of the resin.

2.3.2 Resin Characterization

Limaye characterized the curing properties of DSM Somos 10120 resin using his PμSLA system. A u-shaped part was used to support a cured thread because it offered easy handling. The part was built with the last layer having a thread cured across the top of the U-shape. The top layer was irradiated for different exposure times for each U-shaped sample.

The cured depth of the thread was measured and plotted against exposure time in order to obtain the working curve of the resin as shown in Fig 2.9. The smallest parts made from this machine had dimensions of 20μm and 6μm in vertical and lateral direction respectively.

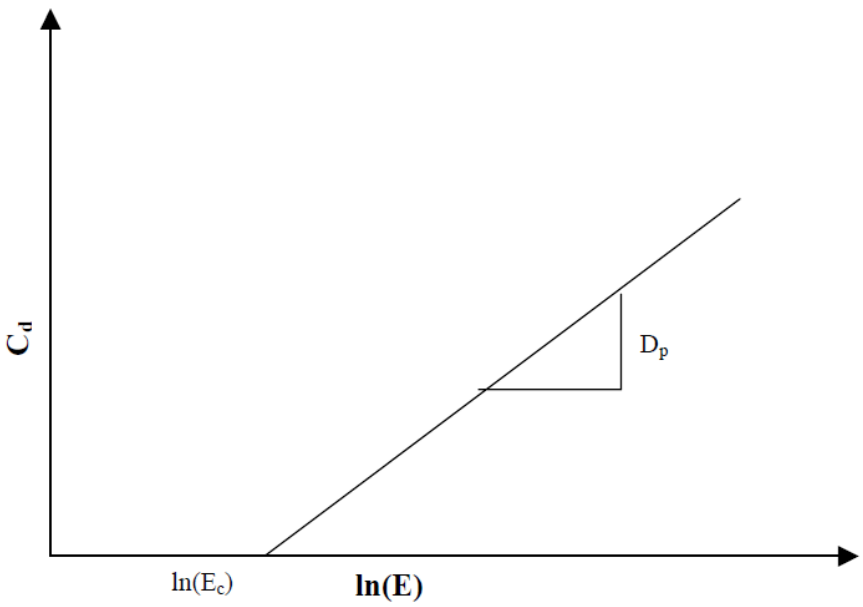

Figure 2.9: Working curve of the resin [16].

2.4 Pekka Lehtinen PμSLA Setup

Pekka Lehtinen has designed and assembled a projection μSLA setup in Aalto University which can produce structure with a few micrometer accuracy [6]. He uses bottom-up based approach in his setup as shown in Fig 2.10.

The main contribution of his work was to construct a bottom-up PμSL system that can be used to fabricate structures with micrometer-sized features. For 3D part manufacturing to be possible the slide show and the z-motor must be properly synchronized. If an image is projected while the motor is still moving, the fabricated structure will be ruined. The program should project images only when the motor is standing still and there is a new layer of fresh resin between the resin vat and the platform.

The movement accuracy of the motorized translation stage must be better than 1μm. The motor movement accuracy as well as the performance of the computer program were tested by curing multiple squares of different sizes upon each other. Thus, it is possible to investigate whether the platform movement corresponds to the input values set into the program and the manufacturing concept is adequate.

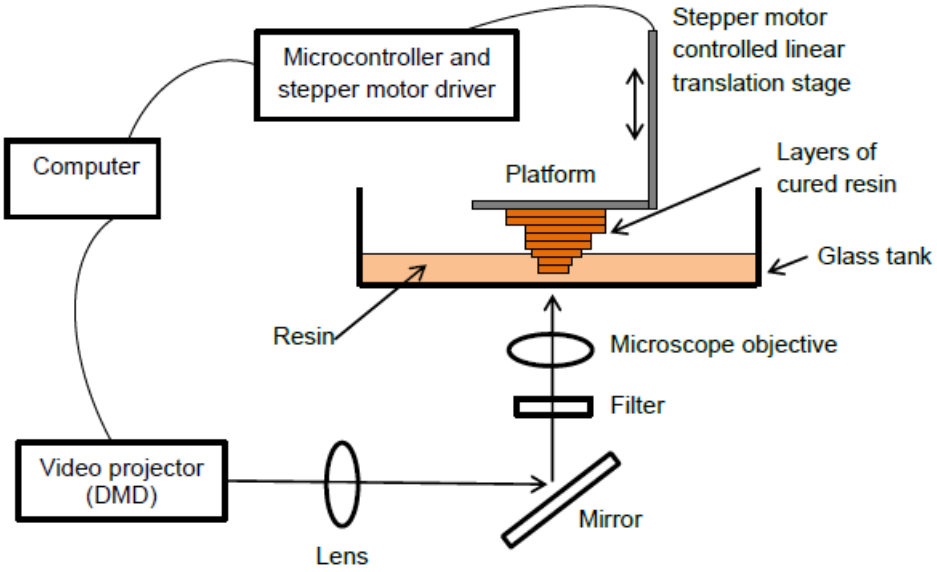

Figure 2.10: An illustration of a bottom-up projection-based microstereolithography apparatus [6].

2.5 CLIP PSLA Setup

Continuous liquid interface production (CLIP) PSLA setup has been introduced by John et al in university of North Carolina at Chapel Hill, USA [17]. The working mechanism of the system has been shown in Fig 2.11. This setup is capable of producing solid parts out of the resin at the rates of hundreds of millimeters per hours which allow parts to be produced in minutes instead of hours. The continuous and fast liquid interface production has been achieved via oxygen-permeable window below the ultraviolet image projection plane, which creates a "dead zone" where photo polymerization is inhibited between the window and the polymerized part.

2.5.1 Working Principle of CLIP

In stereolithography, the oxygen inhibition of free radical polymerization is a widely encountered obstacle to the photo polymerizing UV-curable resins. Oxygen can either quench the photo excited photo initiator or create peroxides by

combining with the free radical from the photo initiator. If these oxygen inhibition pathways can be avoided, efficient initiation and propagation of polymer chains will result.

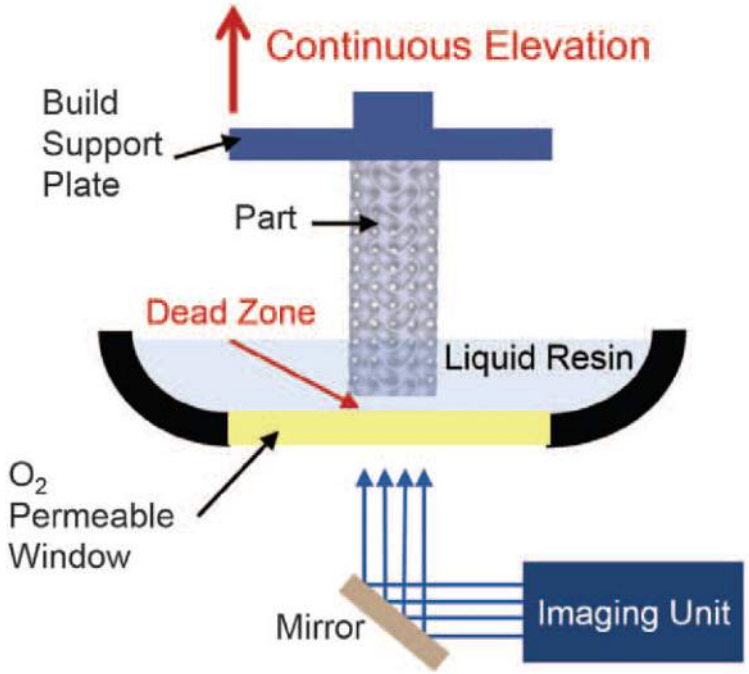

Figure 2.11: Schematic of CLIP printer [17].

Establishing an oxygen-inhibited dead zone is fundamental to the CLIP process. CLIP uses an amorphous fluoropolymer window (Teflon AF 2400) with excellent oxygen permeability(OP). However, OP is a parameter of contact lens which express the ability of the material to let oxygen reach the eye by diffusion. Hence, in this case, this window allows a small amount of oxygen to enter, creating a dead zone where the curing process cannot proceed. As a result, the dead zone maintains a liquid interface directly above it. This dead zone is a thin uncured liquid layer between the window and the cured part surface. In this setup a dead zone thickness on the order of tens of micrometers has been show via judicious selection of control parameters such as photon flux, resin optical and curing properties. The relation of the dead zone thickness has been shown in Equation 2.6

$$DZT = C\left(\frac{\Phi_0 \alpha_{PI}}{D_{c0}}\right)^{-0.5} \tag{2.6}$$

where:
DZT = Dead zone thickness

Φ_0 = The number of incident photons at the image plane per area per time.
α_{PI} = The product of photo initiator concentration and the wavelength-dependent absorptivity.
D_{c0} = The resin reactivity of a monomer-photo initiator combination.
C = Proportionality Constant

Dead zone thickness measurements using a differential thickness technique demonstrate the importance of both oxygen supply and oxygen permeability of the window in establishing the dead zone. The dead zone thickness when pure oxygen is used below the window is about twice the thickness when air is used, with the dead zone becoming thinner as the incident photon flux increases as shown in Fig 2.12. When nitrogen is used below the window, the dead zone vanishes. A dead zone also does not form when Teflon AF 2400 is replaced by a material with very poor oxygen permeability, such as glass or polyethylene, even if oxygen is present below the window. Without a suitable dead zone, continuous part production is not possible.

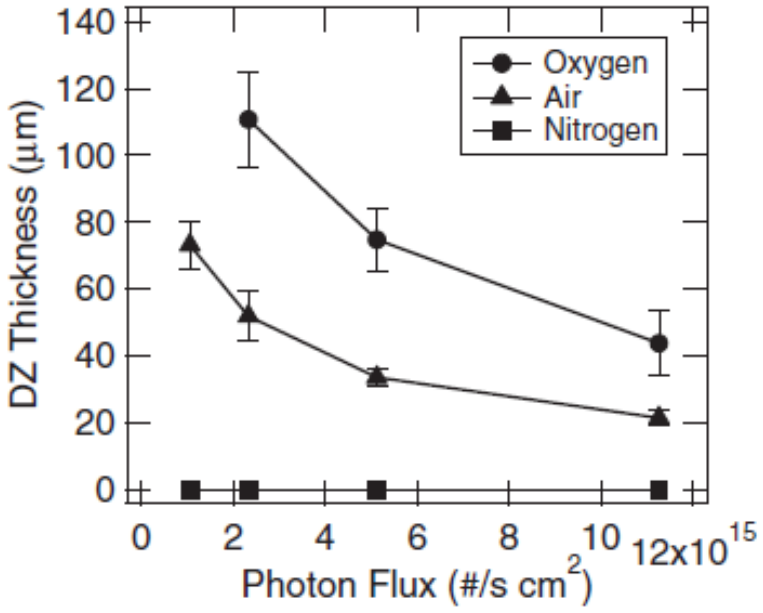

Figure 2.12: Dead Zone thickness for oxygen, air and Nitrogen [17].

2.5.2 CLIP Production Example

The gyroid and argyle structures as shown in Fig 2.13 were printed at 500 mm/hour, reaching a height of 5 cm in less than 10 min. Also, a ramp test patterns has been produced with the same print speed at different slicing layer thickness($100\mu m$, $25\mu m$ and $1\mu m$) as shown in Fig 2.13. At slicing thickness $100\mu m$ the surface quality of the part is not a good and the final part look like layer by layer production. However, as the slicing layer thickness is decreased the surface quality of the part get better and at layer thickness $1\mu m$ the surface is smooth.

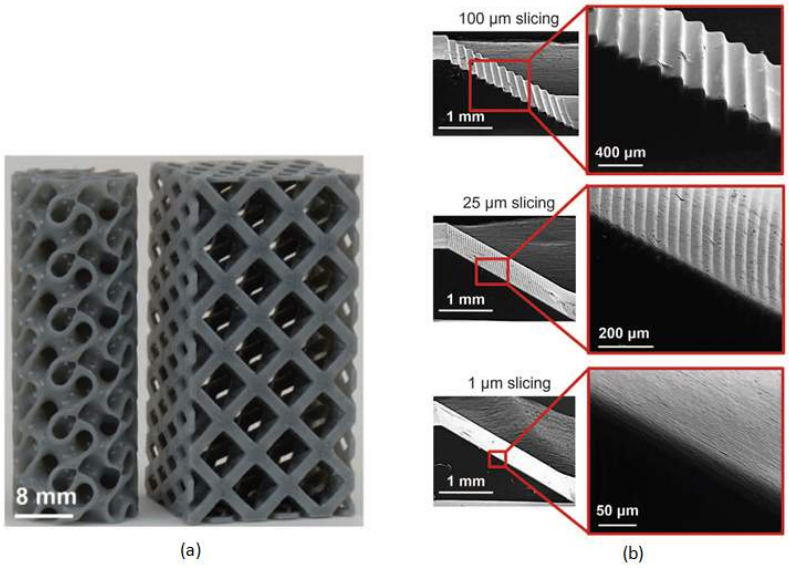

Figure 2.13: (a)Resulting parts via CLIP, a gyroid (left) and an argyle (right), were elevated at print speeds of 500 mm/ hour (movies S1 and S2). (b) Ramp test patterns produced at the same print speed regardless of 3D model slicing thickness ($100\mu m$, $25\mu m$, and $1\mu m$) [17].

2.6 Summary

There were two approaches that had been used for fabrication of a part in stereo lithography process. i) Top-down approach , ii) bottom-up approach.
Every type has its own advantages and disadvantages. The summary of the build setups has been shown in Table 2.1. All the setups(except CLIP) are producing

PμSLA Printers	**Sun.et PμSLA**	**Hadiposespito PμSLA**	**Limaye PμSLA**	**Pekka Lehtinen PμSLA**	**CLIP PSLA**
UV light Source	Mercury lamp	Mercury lamp	Mercury lamp	Video Projector	Video Projector
Type of Translation Stage(TS)	Motorized	PC-controlled three axis micro-stage	Translation Translation	Stepper Motor	N/A
Resolution of the (TS)	0.1 μm	30 nm	N/A	5μm	Below 100μm
Type of Production	Layer by layer Production	Layer by layer Production	Layer by layer Production	Layer by layer Production	Layerless Production
Fabrication Approach	Top to down	Top to down	Top to down	Bottom to up	Bottom to up
Lateral Resolution	N/A	20μm	20μm	N/A	N/A
Chemical Resin	Commercial	Commercial	commercial	commercial	N/A
Main contribution	Development of PμSLA setup and its process modling	Improve the existing setup of PμSLA and did resin characterization	Development of PμSLA setup model its process and resin characterization	PμSLA setup was build and computer programming to run it.	A fast PSLA setup has been build that can produce layerless production.

Table 2.1: Summary of the PμSLA setups.

parts using Layer by layer approach which have certain disadvantages like surface quality of the produced parts.

In this thesis, an in-house projection based stereo lithography system has been developed in which the fabrication of the part is layerless which improve the surface quality of the final part. The setup has been established on top to down approach base production in which DLP projector is used as UV light source. In chapter 3, the detailed assembly and modeling of the setup has been explained.

Chapter 3

In-House DLP Based PSLA Setup

A "In-House" setup of digital light processing (DLP) based projection stereo lithography has been established. It is top down based stereolithography process as shown in Fig 3.1. The main difference of the build printer compared to others is the capability of producing layerless part with good surface finish due to coordinated continous movement in the vertical axis. In the established system, DLP Lightcrafter has been used instead of laser beam system for curing the chemical resin. The working principle of this setup has been shown in Fig 3.1.

DLP base stereolithography system cost less as compare to the typical stereolithography system [18]. Pekka Lehtinen design Projection microstereolithography setup with a DMD chip is constructed that were controlled by computer code during the entire manufacturing process [6]. However, in this setup the DMD chip is already attached inside the DLP projector that is controlled by a controller. The detail of the assembly of this setup has been discuss in the following section.

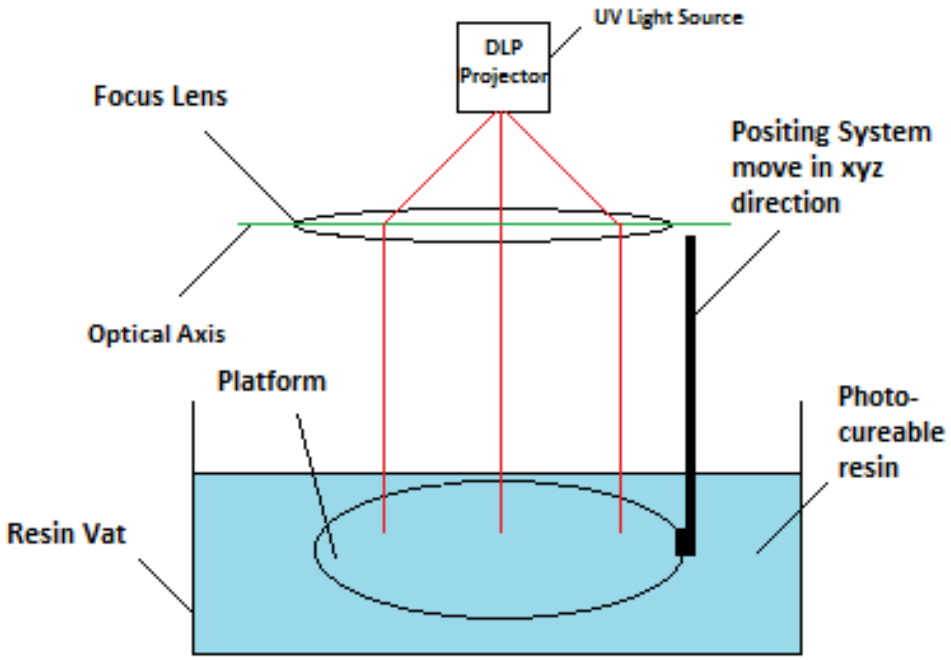

Figure 3.1: Basic Working Principle of DLP based PSL setup develop in Bilkent University.

3.1 Assembly of components

3.1.1 DLP Light Crafter Evaluation Module (EVM)

DLP LightCrafter (EVM) projector has been purchased from Texas Instruments Semiconductor manufacturing company. It is used as a projected light source for industrial, medical and scientific applications. It has a 0.3 WVGA chipset which provides different function such as structured light pattern projection, intelligent lighting, wavelength selection and portable display [19]. Also a DLP-3000 digital micro mirror device (DMD) of 0.3-inch is vertically mounted at the end of the light source for projecting the specific portion of the image. It contains 415872 mirrors arranged in a 608 by 684 with the diamond pattern geometry as shown in Fig 3.2. DC power supply has been used as a power source to supply power to the DLP projector and the voltage that is recommended by the Texas Instrument is 5V.

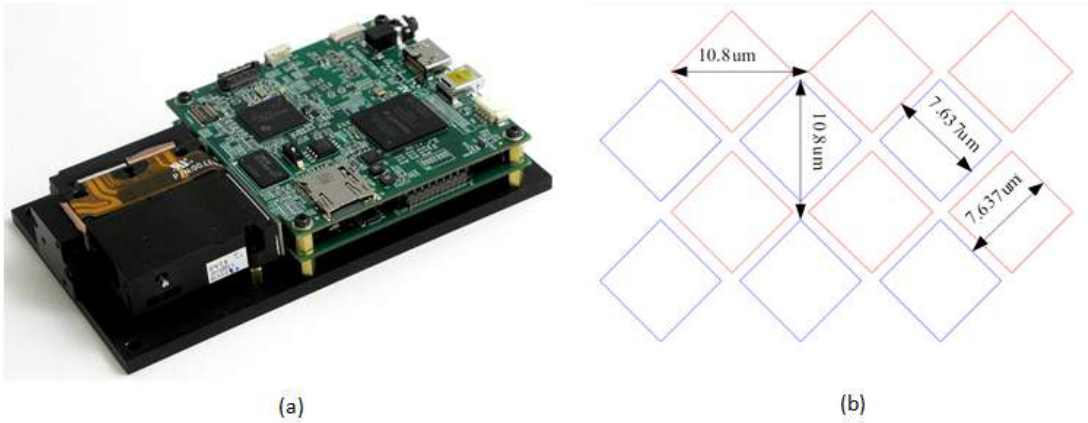

Figure 3.2: (a) DLP Light Crafter (b) 0.3-inch DLP-3000 DMD [19].

The detail about the DLP light crafter components is available in Appendix A. Also the dimensions of the DLP projector has been shown in Fig A.1.

3.1.2 Focusing lens

The basic idea of using lens in front of DLP Projector is to get better quality image onto the platform.

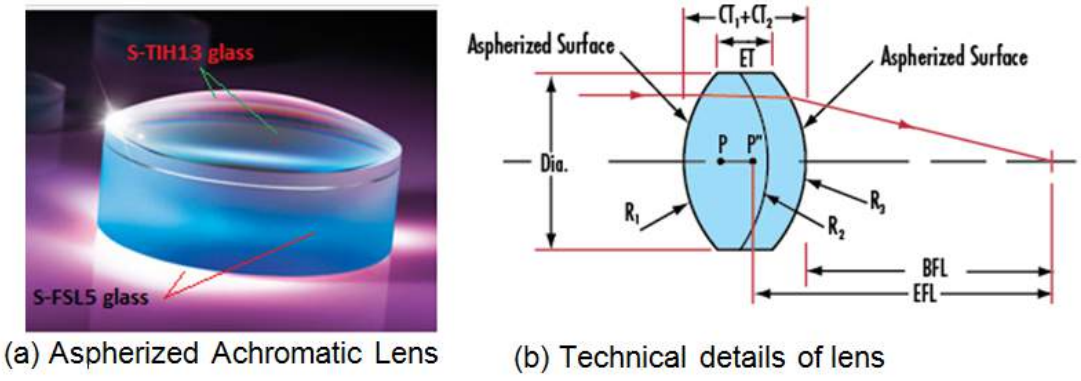

Figure 3.3: Overview of Aspherized Achromatic Lens [20].

Aspheric lenses have been used for converging the projected light on the platform. These lenses bridge the gap between colour-corrected achromats and spherical aberration corrected aspheres, resulting in cost effective, colour corrected aspheric components [20]. The flat part of the lens is made from S-FSL5 glass

Property	Value	Property	Value
Diameter (mm)	25	Center Thickness CT1 (mm)	9
Diameter Tolerance(mm)	0.00-0.05	Center Thickness CT2 (mm)	2.5
Effective Focal Length EFL(mm)	50	Radius 1(mm)	28.6
Clear Aperture (%)	90	Radius 2 (mm) (mm)	31
Back Focal Length BFL(mm)	44.08	Radius 3(mm)	-66
Surface Quality	40-20	Operating Temperature(°C)	-20°C to 80°C
Edge Thickness ET(mm)	7.52	Numerical Aperture(NA)	0.255
Wavelength Range(nm)	425-675	Type	Achromatic lens

Table 3.1: Specification of achromatic lens [20].

while the covex shape part is made from S-TIH13 glass as shown in Fig 3.3(a). The wavelength range of the coating is also matched with the DLP projector for not losing the near-UV region light which enables curing. The technical detail about the lens has been shown in Fig 3.3(b) and in Table 3.1 that represents the specification of the achromatic lens.

3.1.3 Positioning System

A positioning system has been used for the movements of the platform in XYZ direction as shown in Fig 3.4. It has outstanding accuracy, position repeatability and in-position stability. Table **??** shows the specification of the positioning system that have been used for platform movement during DLP stereolithography process. Newport M-IG-22-2 model plate has been used as a base plate for this positioning system. The cad design of the positioning system on the base plate has been shown in Fig 3.4.

The maximum positive travel of the positioning system in XYZ direction is 30

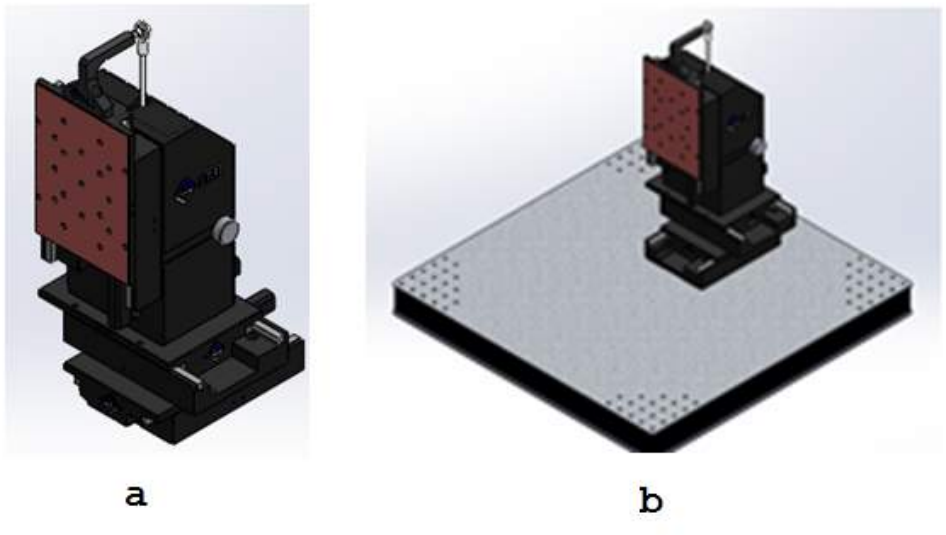

Figure 3.4: (a)Positioning system for platform movement and (b) Assembly with baseplate .

mm and similar for negative XYZ direction which lead to total 60 mm travel in one axis direction.

3.1.4 Final Assembly of the DLP based PSL Setup

The final assembly of these components has been made using supporting structure as shown in Fig 3.5. The build setup has been shown in Fig 3.6 and Fig 3.8 which shows the details of the designed setup. The DLP Projector has been connected with the computer via USB and HDMI cable. The USB cable is require to connect the projector with the system while HDMI cable has been used to project the desired image on the platform.

3.2 Working Principle of DLP based Projection Stereolithography

The process starts with the design of the desired part in CAD software (e.g. Solidworks) which is exported to slicing software to obtain sliced layer information

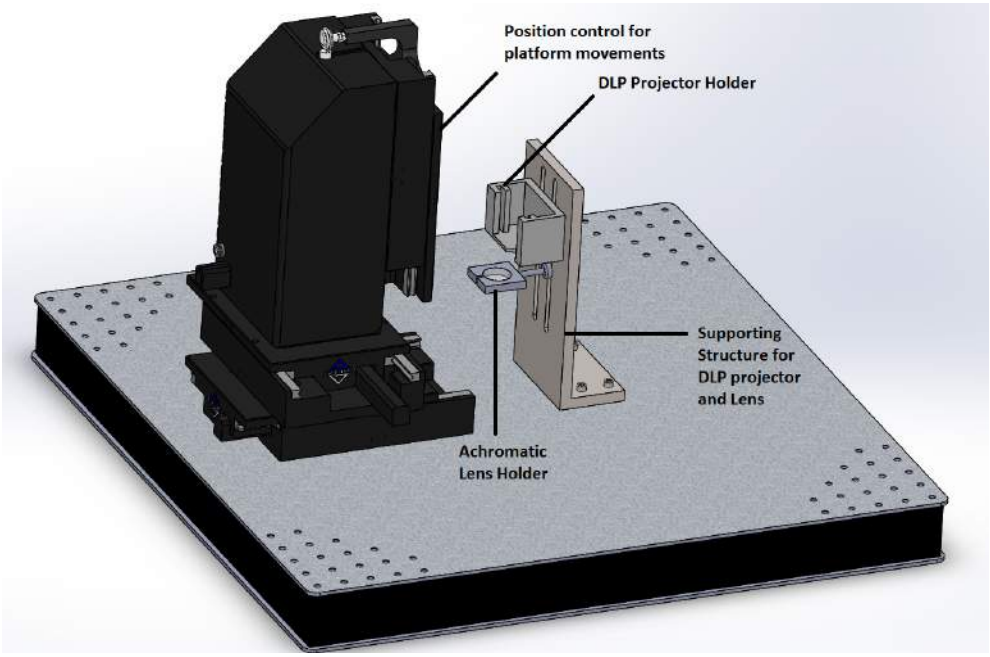

Figure 3.5: CAD Assembly of the DLP based PSL setup

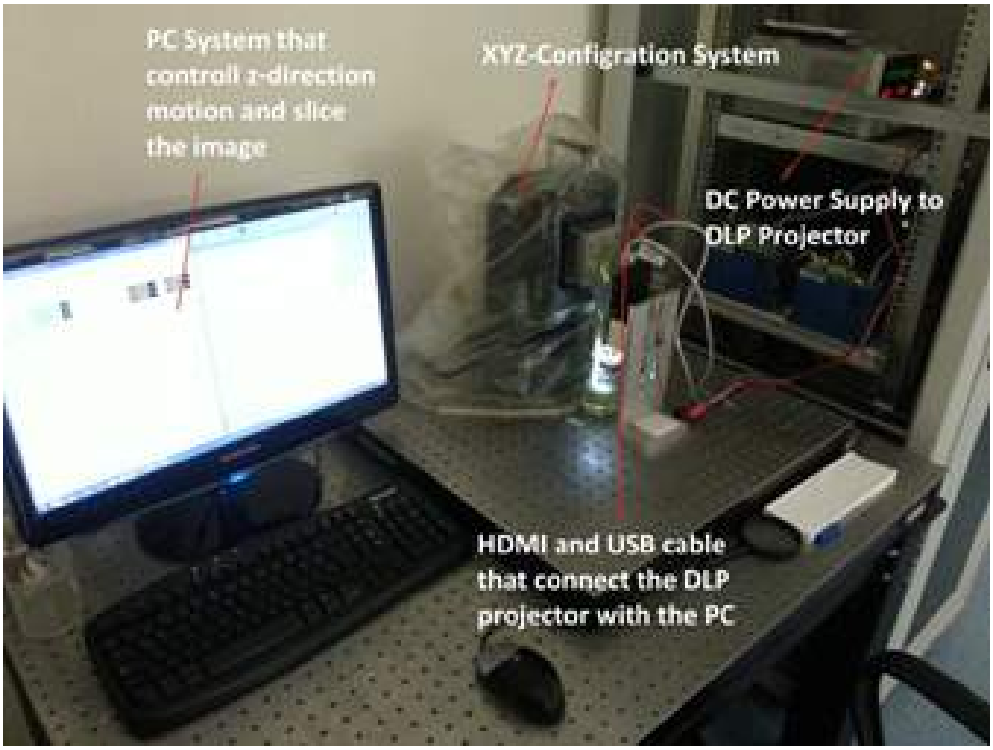

Figure 3.6: Build Setup of DLP based PSLA

in STL format. Layer thickness has a great influence on the mechanical properties of the part in stereo lithography [21]. Flashpoint slicing software has been used for this purposes [22]. Using this software, the layer thickness of 0.001 millimeter can be achieved. Slice images are projected one by one to the platform surface as shown in the Fig 4.11.

At the start, platform is dipped into the liquid resin by leaving desired amount of the liquid above the surface. When the light rays hits the surface, the resin solidifies and forms the first built layer. By providing a velocity command to the system in z-direction, the platform starts to move down into the liquid, which bring more liquid to the upper side of the created layer for the solidification of the next layer. Since the exposure time of each slice is controlled through the software, the number of slices and exposure time for a single slice can be adjusted in order to finish the production with desired number of layers and dimensions. When the projected image of the layers is finished, the part is completed and dipped part is taken out. The part is cleaned with de-ionized water, isopropyl alcohol mixture and then carefully removed from the workplace [23].

The working setup for the production purposes has been explained in Fig 3.6. The detail view of DLP setup has been shown in Fig 3.8.

In this setup, there are four parameters that can be controlled. The speed of the linear stage in Z-direction, light intensity (LI) of the DLP projector, focusing lens that is used for converging the light and chemical composition of the resin. There is an experimental study has been done to find the optimum parameters of light intensity and speed of the z-axis for high aspect ratio structures.

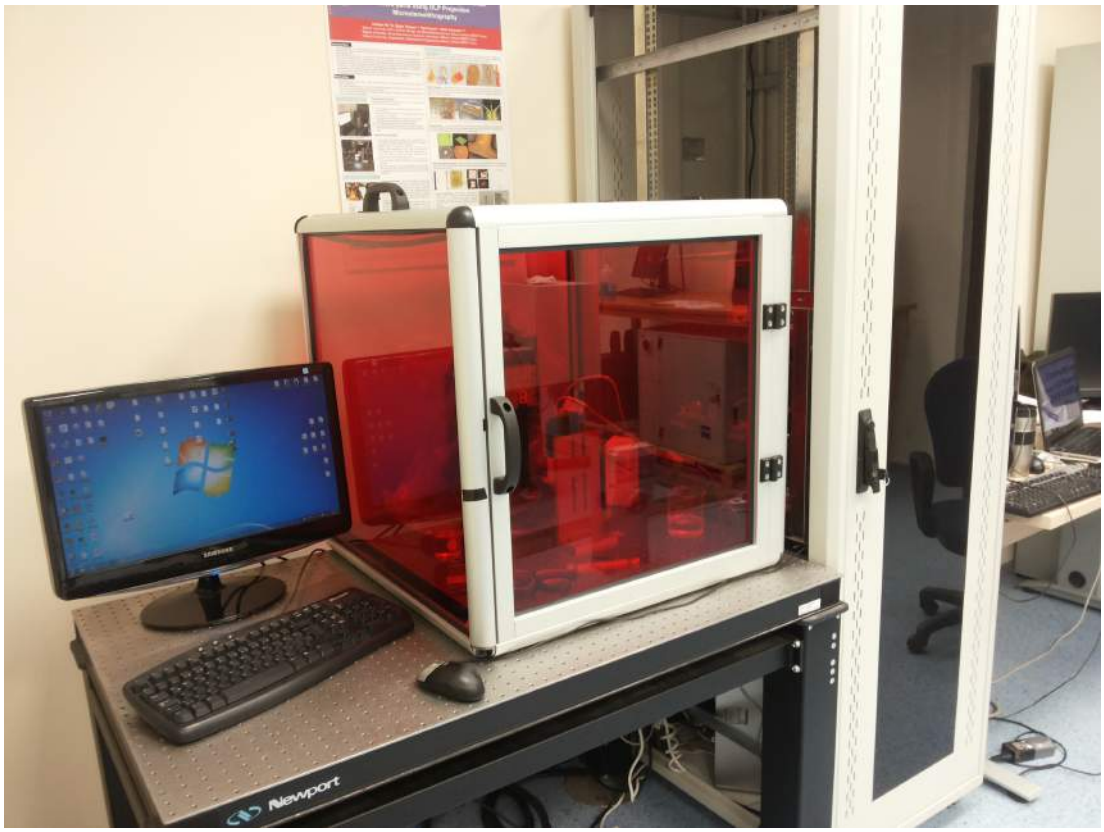

Figure 3.7: DLP based Projection Stereolithography (PSLA) Setup

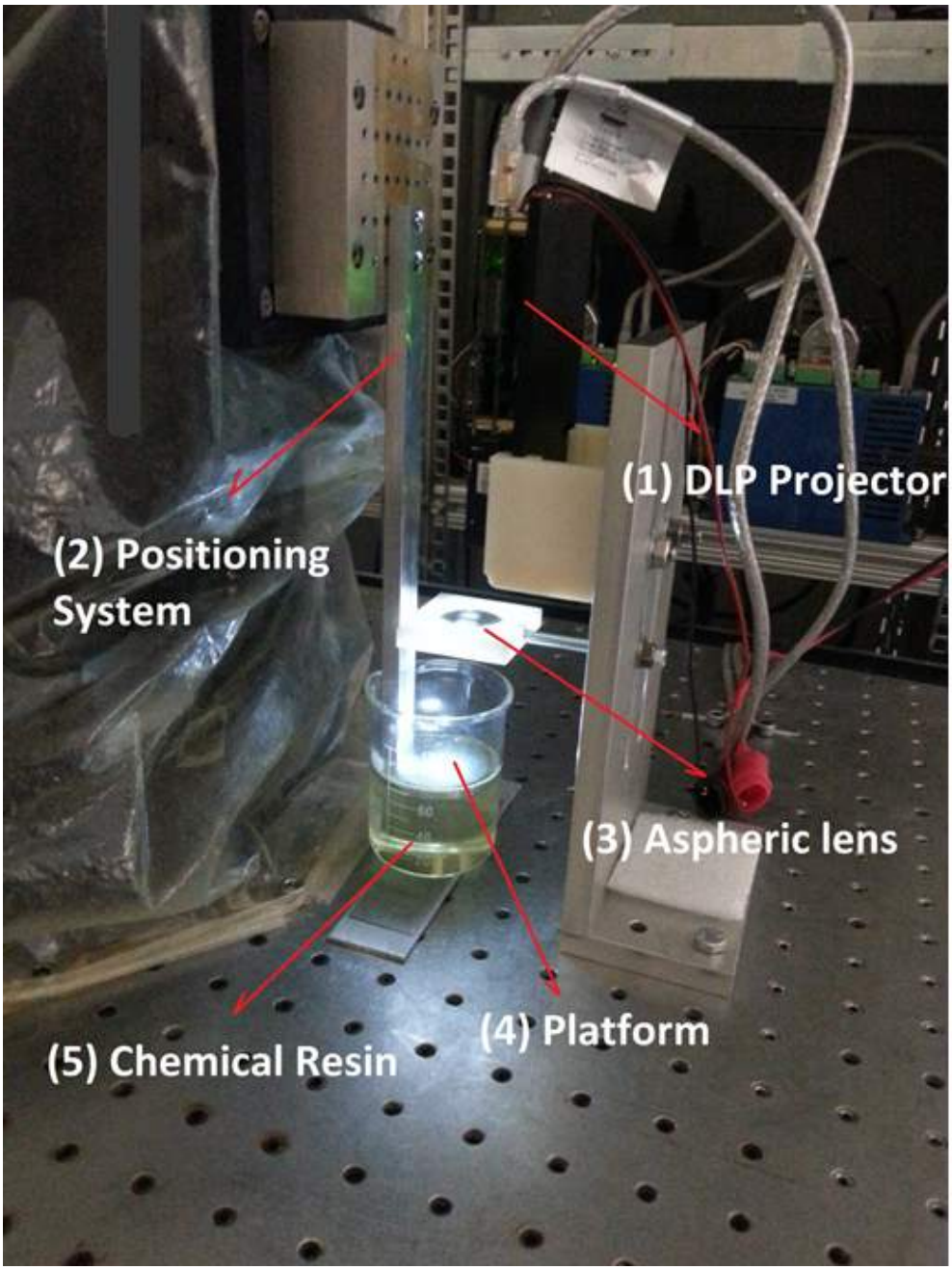

Figure 3.8: Detail view of DLP based PSLA Working mechanism

3.3 Investigation of Process parameters

An experimental study has been performed to investigate the influence of speed and light intensity on the production while the chemical composition of the resin and optical lens of the system is kept same during that study.

In order to find the process parameters of the system, a square shaped pillar design is considered. Initial production trials were performed with the DLP stereo lithography system. After producing the pillar, it is compared with the original design in terms of width, volume and flatness of the upper top surface as shown in Fig 3.9. Optimum process parameters must be known prior to fabrication so that high accuracy can be achieved with minimum trials.

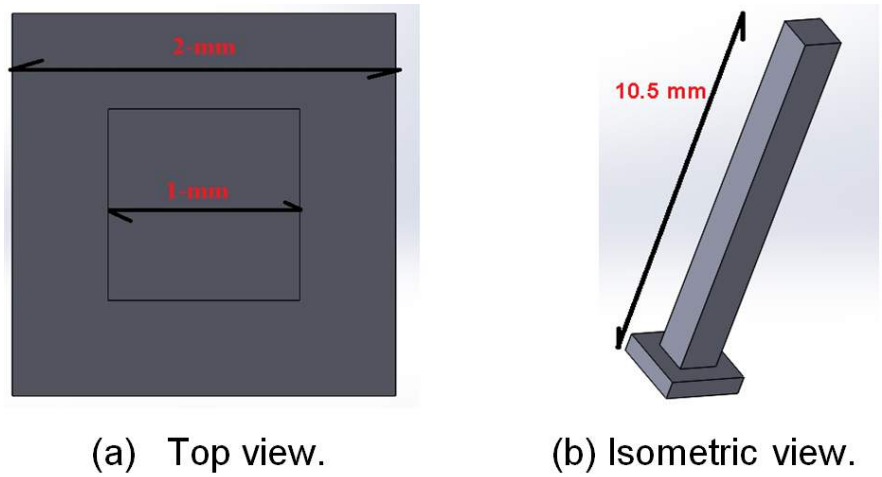

Figure 3.9: CAD design of the tower

Only light intensity and speed of the Z axis were considered as process parameters. The low level values of speed and light intensity are 5 nm/s and 1 mA and high level values are 30 nm/s and 274 mA, respectively. Nine trials have been done with three levels of factors as shown in Table 3.2. Using DOE, it is expected to find the process improvement direction and eventually find the optimal process parameters.

No of Obs	Speed	Light Intensity
1	5	1
2	5	137
3	5	274
4	15	1
5	15	137
6	15	274
7	30	1
8	30	137
9	30	274

Table 3.2: Design of experiment representations

3.3.1 Experiment

All trials have been performed according to DOE given in Table 3.2 and nine pillars were fabricated through DLP based projection stereolithography system as shown in Fig 3.10. Isopropyl alcohol was used to clean the pillars after the production [23]. In order to reduce systematic errors, experiments were repeated

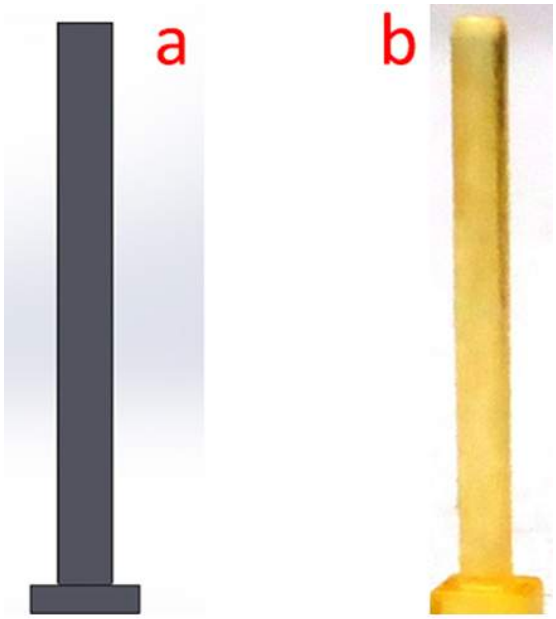

Figure 3.10: (a) Tower CAD design, (b) Fabricated tower

four times and then the average values of width, volume and top surface flatness have been recorded. And new DOE levels has been decided based on these

parameters which gave less errors and expected to provide better error results.

3.3.1.1 Measurements

In this study, optical (Keyence VHX) and laser scanning (Keyence VKX) microscopes as shown in Fig 3.11 has been used for measuring the dimensions of the cured part. A digital microscope has been used to measure the width of the

Figure 3.11: (a) Keyence VHX Optical Microscope, (b) Keyence VK-X100 Laser Microscope

tower and laser microscope is used to measure the volume and flatness of the top side of the pillar as shown in Fig 3.12 and Fig 3.13. In order to measure the flatness of the surface, a flat surface of steel part has been captured first and then compared with the fabricated part surface. For volume measurement, top 500 micron of the designed tower has been compared with top 500 micron of the fabricated tower. The errors between them have been recorded .

3.3.2 Results of DOE

The average % error in width, volume and flatness has been showed in Fig 3.14. The x-axis in Fig 3.14 shows the speed of Z axis in nanometer per second (nm/s). From the results, it can be concluded that error percentage in width will increase as the speed of the Z axis increases. Maximum light intensity (274 mA) with

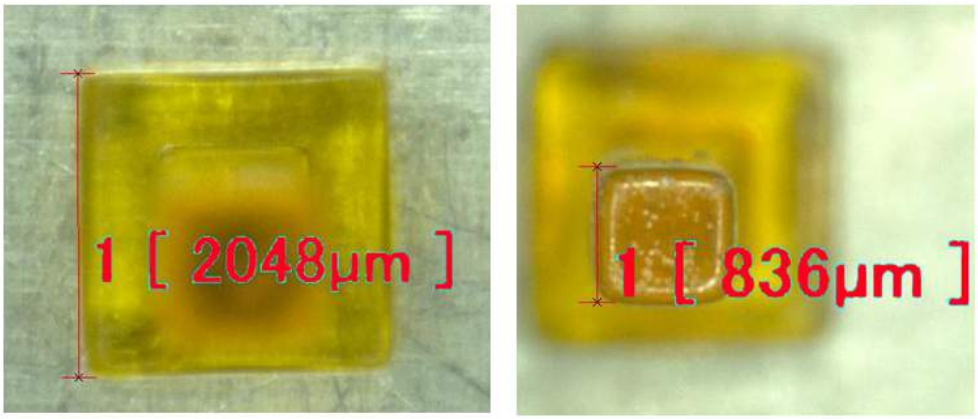

(a) Bottom side of square. (b) Top side of square.

Figure 3.12: Digital microscope images of the fabricated tower shape.

15 nm/s seems to be yield better suitable process parameters considering the width. For volumetric error and flatness, low level speed and high light intensity parameters yield better results. It must be noted that the error percentage is around 32% for the most suitable parameters. Based on these results, a second set of experiments were designed by considering speed range of 5 to 15 nm/s and light intensity values were kept same.

3.3.3 Second Phase of DOE

In the new DOE same levels of light intensity have been considered which are 1,137 and 274 mA but for speed the new levels have been selected which are 6 ,8 and 10 nm/s on the basis of the results of previous DOE and new design of experiments have been designed as shown in Fig 3.15. All the trials have been performed and nine new pillars have been produced. In order to measure the % error in width, volume and flatness the same procedure has been followed as it was done for first set of experiments.

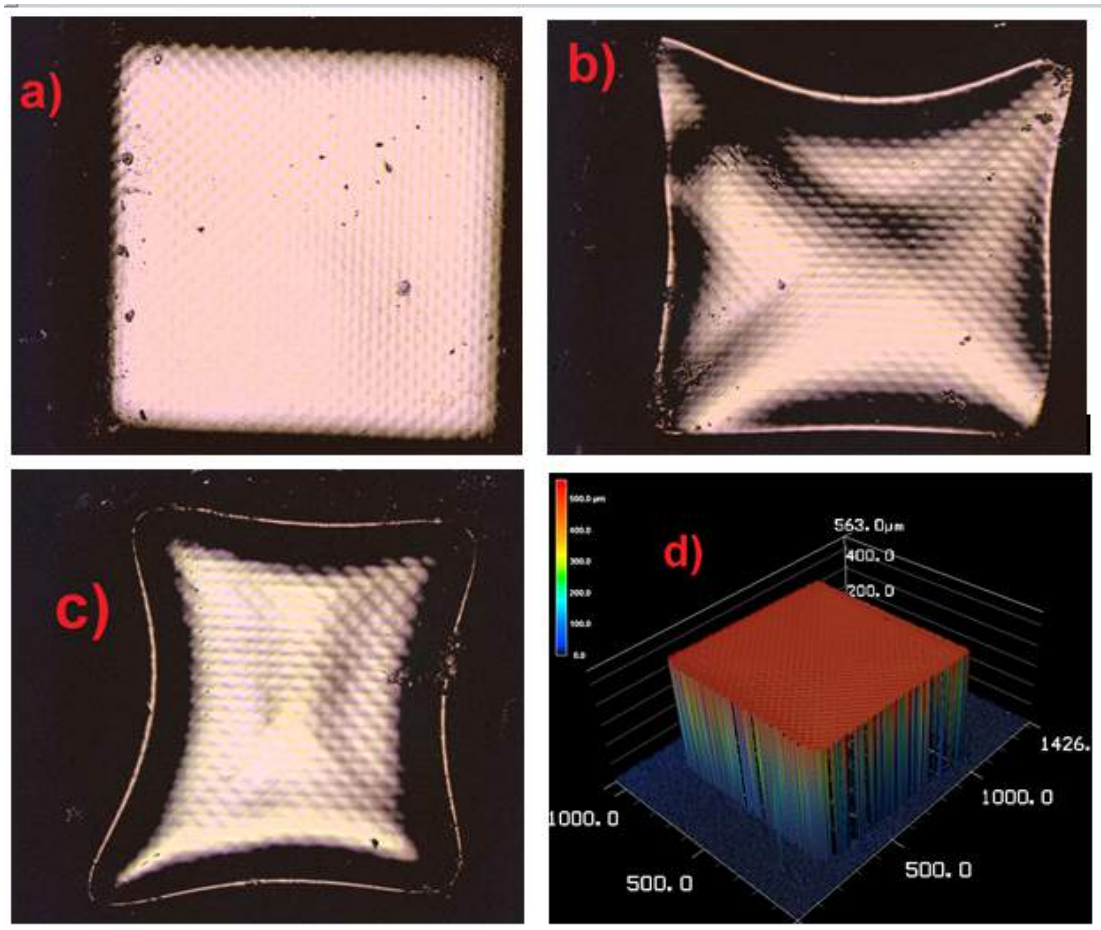

Figure 3.13: Laser microscope images of the top surface of the square for the comparisons purpose of flatness and volume with the designed tower.(a) At speed 5 with LI 137.(b) At speed 15 with LI 137.(c) At speed 30 with LI 137.(d) 3-D image of the top

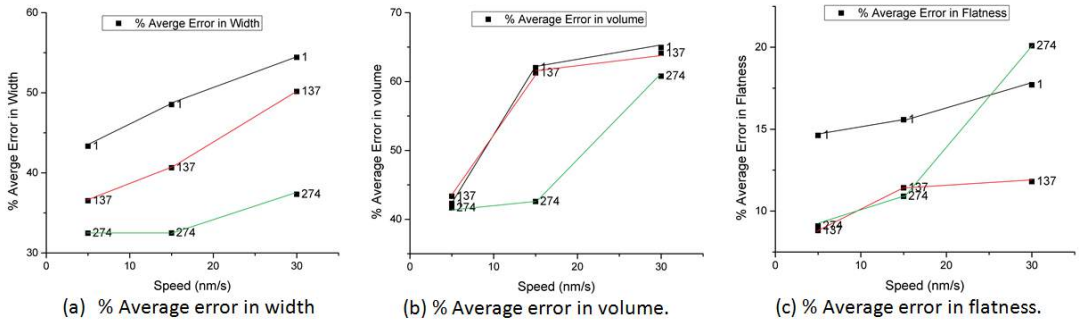

Figure 3.14: Average % error with different combinations of light intensity and speed.

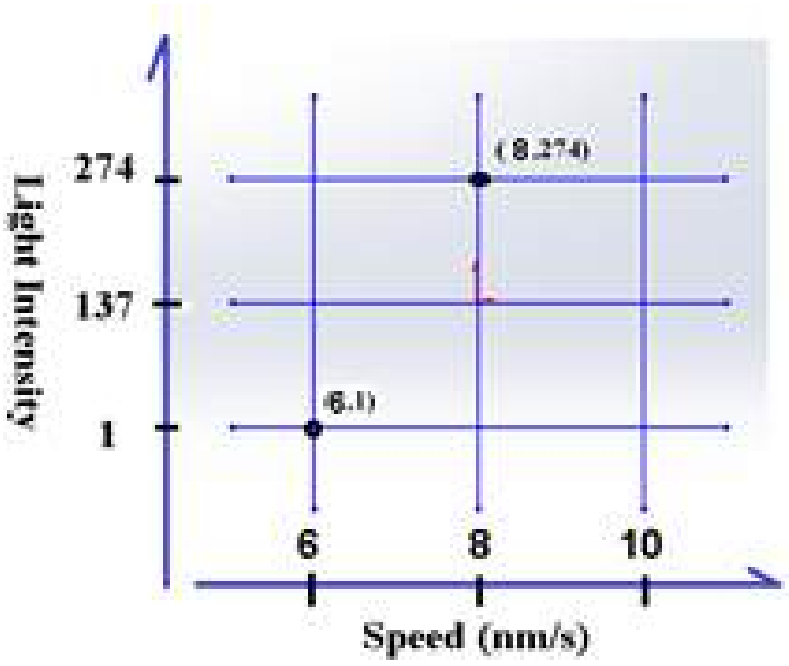

Figure 3.15: Graphical representation of new DOE.

3.3.4 Results of the second phase of DOE

The average error value of the width, volume and flatness has been showed in Fig 3.16. The minimum % error in width and volume has been found at speed

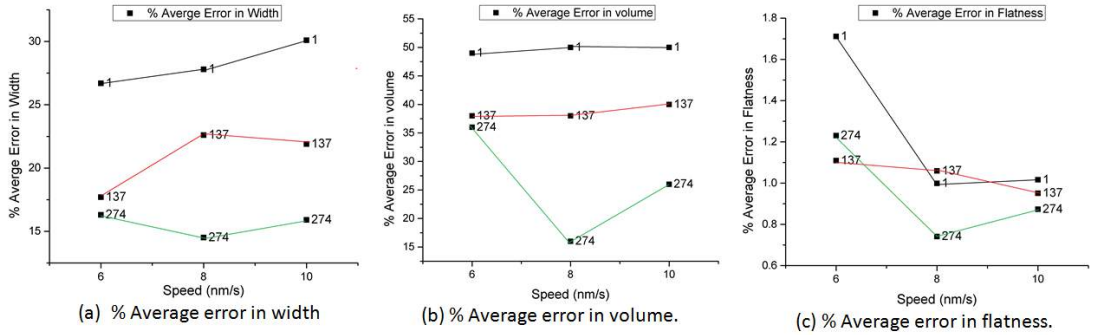

Figure 3.16: Average % error with different combinations of light intensity and speed.

value of 8 nm/s with light intensity of 274 mA. For flatness, at 6 nm/s produced better results were obtained. At light intensity of 274 mA, the error is around 16%. From all these experiments, it can be concluded that speed 8 nm/s with light intensity 274 mA gives the best production. At this condition, 14.5% error

in width, 16% error in volume and 0.741% error in flatness were obtained. The experimental data sheet has been attached in Appendix B as shown in Fig B.1 and Fig B.2.

3.3.5 Two-Way ANOVA Test

In order to see the significance importance of LI and speed in % average error in Width, Volume and Flatness two-way analysis of variance (ANOVA) test has been performed and examine the p-value. The 95% confidence interval has been set and alpha value is 0.05. If the p-value is less than alpha value than its means that the factor is significant and our null hypothesis is true and vice versa. The test has been performed using Minitab and the results of it have been attached in Appendix B Fig B.3. As P-values in all the cases is less than 0.05 which lead us to conclude that the LI and speed has significance importance in % average error in width, volume and flatness.

3.3.6 Role of Optics Lens

If we look at the error that has been received after the improved DOE results than it suggest to set another DOE as the errors is above 10%. However, instead of going for another DOE, this time the optical lens has been change and achromatic and aspherized lens has been used to see the effect on the results. The same experiment has been repeated with the achromatic aspherized lens. The optical lens play a vital role in terms of the dimensional accuracy of the fabricated part. The % errors of the parameters started decreasing with the use of aspherical and new percentage errors for width, volume and flatness became 4.6%, 10% and 0.559% at speed 8 with LI 274.

Optical lens plays a vital role in terms of the dimensional accuracy of the fabricated part. As achromatic lenses increases the level of colour correction for the projected image on the platform while spherical aberrations are corrected with aspheric shape. The other lens used was a spherical one which had an effect on the conformity of the projected image because of the aberration. For the aspherical lens, wavelength range of the coating is also matched with the DLP

projector for not losing the near-UV region light which enables curing. Hence the effect of optical lens on the % error of the parameters was significant. Detailed explanation about the optics is given in the next chapter.

3.4 Summary

The optimum parameters of the system has been find using a square shaped pillar via design of experiments technique. There is a need for an image model which can predict the size of the part that is going to be fabricate and what is the exposure time require to cure the part.

Chapter 4

Image Formulation and Cure Modeling of the Process

4.1 Fundamentals of Image Formation

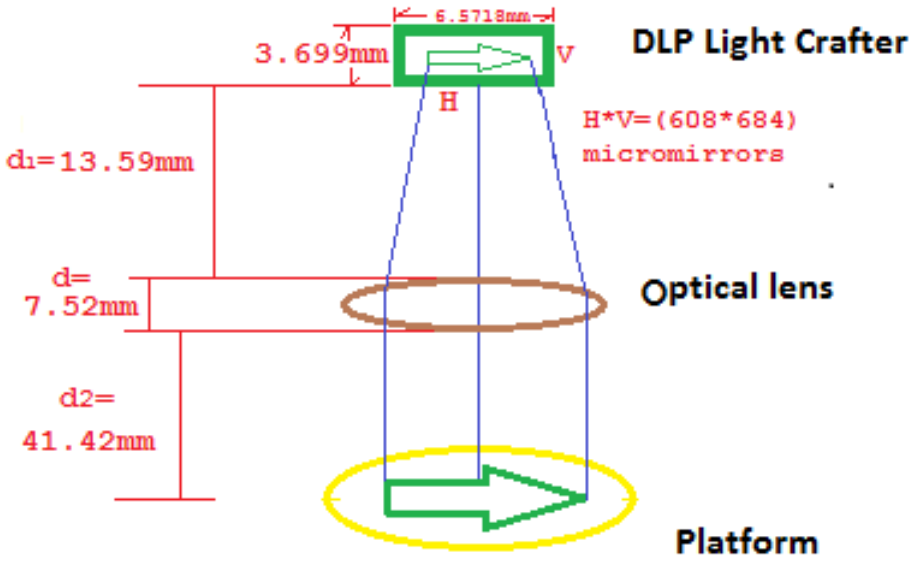

Figure 4.1: Projection of image from DLP projector to the platform with dimensions.

In this section, the optics behind the image formation on the platform and the size of the projected image has been model for DLP based Projection Stereo lithography. The working mechanism of image formation has been shown in Fig 4.1.
where:
d_1 = Object distance.
d_2 = Image distance.
d = lens diameter.
H = Horizontal dimensions of digital micro mirrors (DMD) device.
V = Vertical dimensions of digital micro mirrors (DMD) device.
H*V=Total no of mirrors in the DMD device.

As the size of single mirror is $7.637\mu m$ and using it the horizontal and vertical dimensions has been found which is equal to H and V respectively. The pixel size of the projected image can be found via following equations.

$$M = d_2/d_1 \tag{4.1}$$

$$I_h = H * M \tag{4.2}$$

$$I_v = V * M \tag{4.3}$$

$$P_s = I_v/640 = I_H/480 \tag{4.4}$$

where:
M = Magnification
I_h = Horizontal Projected Image size
I_v = Vertical Projected Image size
P_s = Pixel size of the Projected Image
The maximum projected image size is $I_h * I_v = 11.1726 * 14.8968mm$.

4.1.1 Projected Image size.

The size of the projected image when all the pixels are illuminating light on the platform can be find via Equation 3.2 and Equation 3.3 because the object size is known in this case. But the object size is not known always, for example if the object size is smaller on the DMD than the image size will also change. As object size is unknown than the projected image size can not be find using above

equations. To solve this issue an empirical study has been done in which the relation between the projected image size and design image size has been found. If we look at the process of image formation on the platform it has been found that the image that we are getting on the platform first has been designed in CAD software and lately has been sliced and projected onto the platform. In this way the relation between projected and designed image can be found.
The process of image projection is:

1. Design a desired image size on the CAD software (solidwork).
2. Convert the CAD file into STL format and slice it into desired number of layers.
3. Project the layer on the platform using DLP projector.
4. Measure the projected image size on the platform.
5. Find a relation between the projected image size and design image size.

4.1.2 Projected Image vs Designed Image

A square of length 45mm has been designed in solidwork to find the relation between projected image size and designed image size. After following the above five steps the relation has been found as shown in Fig 4.2.

1mm projected image size in platform = 4.511802941mm design image size in solidworks. The matlab codes in Appendix C-2 has been written in order to find the projected image size .

4.2 Irradiance measurement

For accurate curing of parts via DLP Projector, it is mandatory to know the irradiance of the DLP Projector that is illuminating at the platform. Irradiance is the radiant flux received by a surface per unit area and spectral irradiance

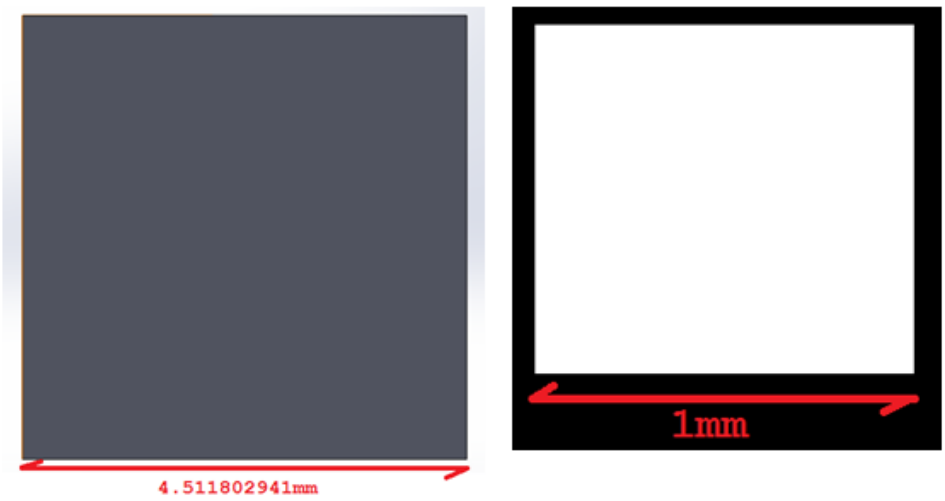

Figure 4.2: Relation between projected image size and designed image size.

is the irradiance of a surface per unit wavelength. Power meter has been used to measure the total irradiance of the DLP Projector. A white circular image spot has been projected on the power meter whose diameter is 11.5mm. The setup has been shown in the Fig 4.3. Total irradiance of the circular image is 30.6mW(milliwatt) that has been measured via power meter as shown in Fig 4.3. As the diameter of the circle is known than using it irradiance per unit area has also been found which is 29.4602 mW/cm^2.

However, as DLP projector has a broadband LED as a source of light that is a combination of red, green and blue light. These light has different wavelength and spectrum that has been shown in Fig 4.4 [24]. Ultraviolet (UV) light is required to cure the chemical resin and among these lights of LED only the blue light has wavelength that is close to the UV wavelength region. The irradiance (29.4602 mW/cm^2) that has been measured via power meter has wavelength of all lights but resin cure mainly at blue light wavelength. Hence the irradiance of the blue light need to be measured for curing the resin accurately. The area under the curve for each light from the spectrum has been calculated to find the irradiance of blue light wavelength.

$$I_b = (I * A_b)/(A_b + A_g + A_r) \tag{4.5}$$

$$I_g = (I * A_g)/(A_b + A_g + A_r) \tag{4.6}$$

$$I_r = (I * A_r)/(A_b + A_g + A_r) \tag{4.7}$$

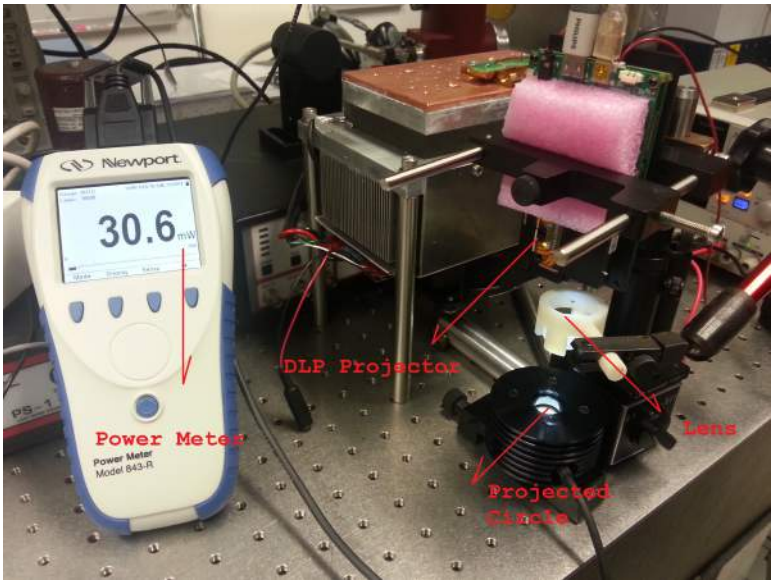

Figure 4.3: DLP Projector irradiance measurement setup.

where:

- A_b= area under the curve for blue light spectrum
- A_g= area under the curve for green light spectrum
- A_r= area under the curve for red light spectrum
- I_b= Irradiance/area for blue light
- I_g= Irradiance/area for green light
- I_r= Irradiance/area for red light
- I= Total irradiance/area measured via power meter

A digitized data has been taken from LED spectrum as shown in Fig C.1 in Appendix C. The area under the curve of each spectrum has been calculated using it. The I_b has been calculated using the above formulas and it has been found around 6.21mW/cm^2. The Matlab code has been written to calculate the irradiance of LED spectrum in Appendix B.

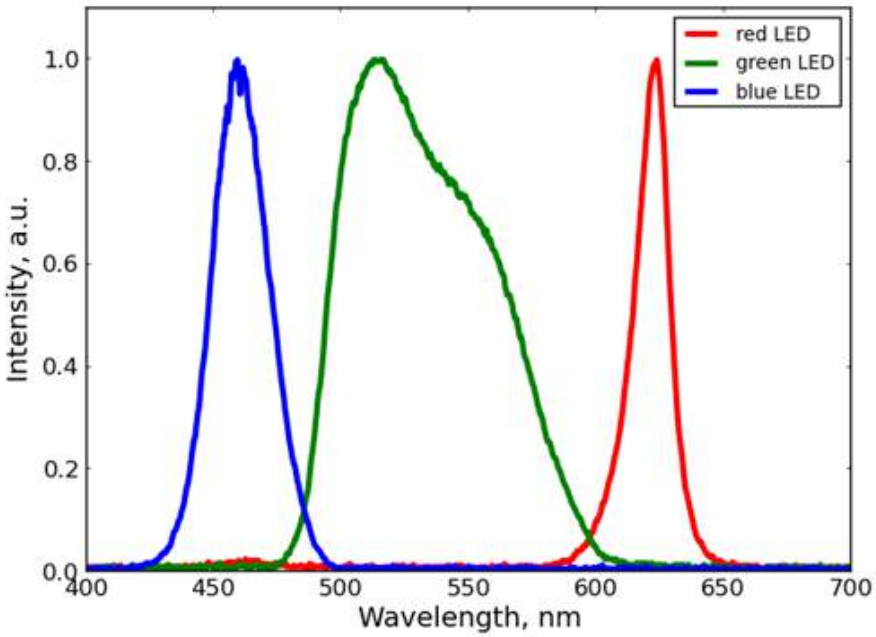

Figure 4.4: Spectrum of the LED inside the DLP Projector. [24]

4.3 Fundamentals of Resin Curing

In this section, the chemistry behind the photo polymerization reactions that occur when a stereo lithography resin cures is presented. Then the expected curing characteristics of a resin are presented along with a chemical explanation to it.

4.3.1 Photo-polymerization

Polymerization is the process of linking small molecules (monomers) into larger molecules (polymers) comprised of many monomer units. Most Stereolithography resins contain the vinyl monomers and acrylate monomers. Vinyl monomers are broadly defined as monomers containing a carbon-carbon double bond. Acrylate monomers are a subset of the vinyl family with the carboxylic acid group (-COOH) attached to the carbon-carbon double bond. For an acrylate resin system, the usual catalyst is a free radical. In Stereolithography, the radical is

generated photo chemically. The source of the photo chemically generated radical is a photo initiator, which reacts with an actinic photon as shown in the photo-polymerization scheme presented in Fig 4.5 . This produces radicals (indicated by a large dot) that catalyze the polymerization process [16]. In the radical for-

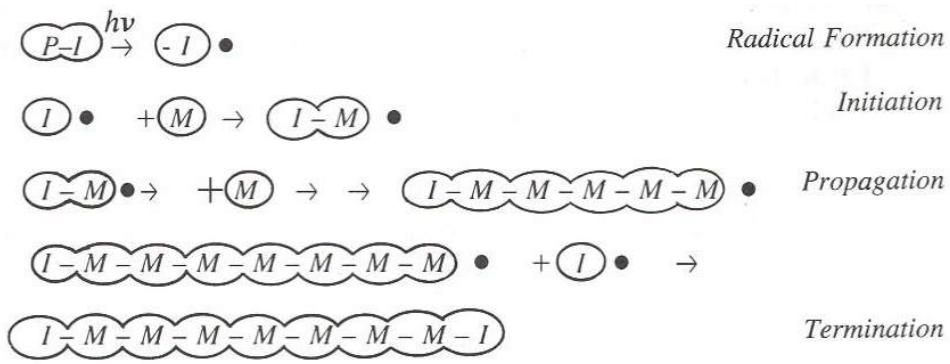

Figure 4.5: Scheme of the photo-polymerization process [16].

mation step , the photo initiator (P-I) is excited by absorption of a photon of appropriate wavelength and produces radicals. In the initiation step this radicals react with the monomer(M) and start making chain. The polymer lengthens by continuous addition of monomers in propagation step. Finally the termination occurs when another radical join this polymer chain.

4.3.1.1 Photocuring

The word curing refers to solidification of a polymeric solution. RadTech North America defines radiation curing in the following manner: "radiation as an energy source to induce the rapid conversion of specially formulated 100% reactive liquids to solids". Curing is achieved in most cases with UV, but in some occasions it is possible to utilize electron beams, X-rays, gamma-rays, visible light, plasmas and microwaves for it [25].

4.3.2 Resin Preparation

In this study commercial and in-house resin has been used for curing purposes. The commercial resins has been purchased from Spot-A materials company which

are Spot-HT and Spot-E while in-house resin has been mixed manually with specific amount of components.

4.3.3 In-House Resin

The compositions of the in-house resin that has been used in this study for fabrication of different parts consist on the following components.

- Polyethylene Glycol Diacrylate (PEGDA)
- Sudan-I
- Phenylbis

Resin has been prepared manually by mixing appropriate amount of each component. PEGDA is main polymer in the resin which diffuses into gel network after specific energy has been exposed.

4.3.3.1 Phenylbis(2,4,6-trimethylbenzoyl)-phosphine oxide

Phenylbis is a photo initiator that discharges free radicals when it absorbs photon(i.e from light source). It causes the monomers in solution to bind and polymerize. The presence of oxygen confines the quantity of free radicals accessible for photo polymerization.

4.3.3.2 Sudan-I

Sudan-I is a photo inhibitor and prevents the exposure dose from penetrating deep into the polymer, which helps in controlling the layer thickness. The concentration of Sudan-I can be adjusted to make thinner or thicker layers. Adding more Sudan-I will make thinner layers because more UV light will be absorbed [26] [27].

4.3.3.3 Mixing of Resin Components

To make the PEGDA solution, combine 98mL of Polyethylene Glycol Diacrylate with 2.00 grams of Phenylbis and 0.005 grams of Sudan I. Add all the chemicals in a bottle after measuring the appropriate amount of each chemical and than put it onto the magnetic mixer for three days. After three days, the resin will be ready for production purposes.

4.3.4 Resin characterization

4.3.4.1 In-House Resin characterization

In order to find the how much resin will cure at specific light intensity the Beer-Lambert law has been used. The relation between the depth of cure (C_d) and the exposure on the resin surface (E) is given by:

$$C_d = D_p ln(E/E_c) \tag{4.8}$$

where E_c and D_p are constant resin parameters and E is the energy that is coming out from the projector to the platform. D_p is the depth in the resin to which the irradiance falls to $(1/e)$ times the irradiance on the resin surface. E_c is the minimum exposure required to initiate the photo-polymerization reactions. The values of E_c and D_p are generally provided by the resin manufacturer side but resin has been mixed manually hence these values need to be find experimentally.

4.3.4.2 Experiments performed to characterize the resin

The following experiments have been performed to plot the working curve of the resin. A polymer thread is photo polymerized, supported on a U-shaped micro-part as shown in Fig4.6. The supporting micro-part is U shaped because it offers rigidity and is easy to handle and place under a microscope [16]. The u-shaped part has been designed in solidwork and than the STL file of it has been transfered to flash point software for slicing purposes. The thread is located approximately at the center of the imaged area of the mask. The thread is cured by exposing it to radiation for different durations of time as shown in Fig 4.7 and Fig 4.8.

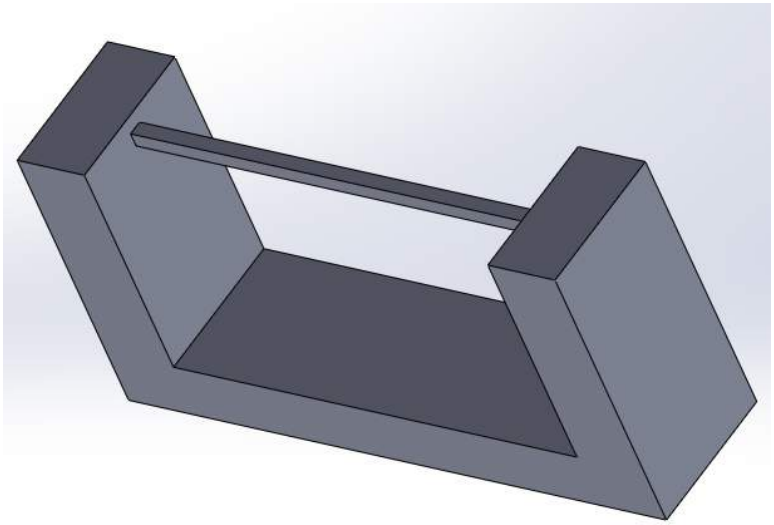

Figure 4.6: CAD Design of Thread for Cure Depth measurement.

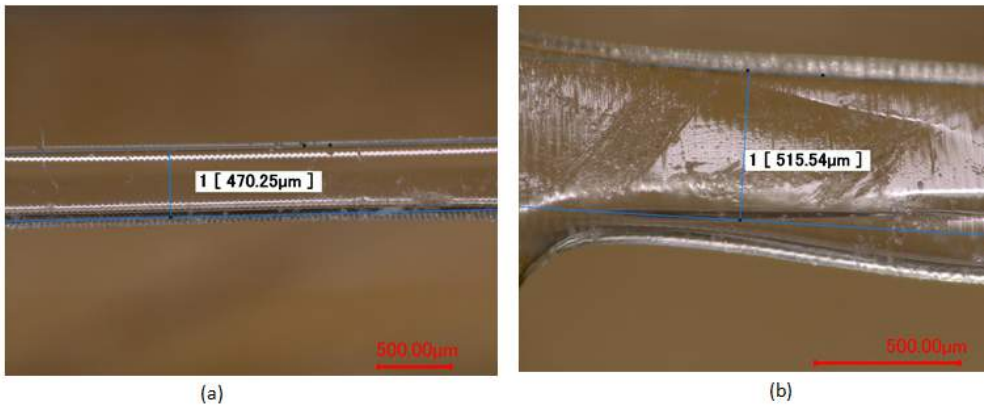

Figure 4.7: Polymer thread cured at (a) 60 sec exposure, (b) 90sec exposure

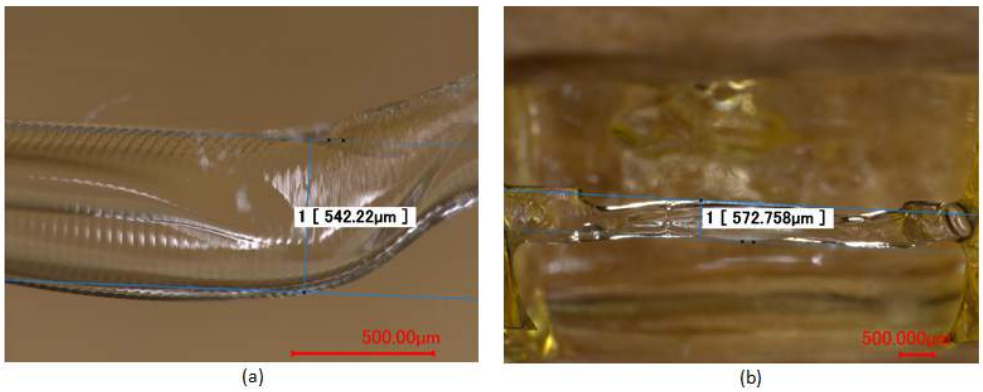

Figure 4.8: Polymer thread cured at (a) 105 sec exposure, (b) 120 sec exposure

The thickness of the thread in the vertical direction is measured and plotted against the time of exposure. As in section 3.2 it has been found that the average irradiance on the image is approximately 6.21mW/cm2. The exposure received by thread is calculated by multiplying the average irradiance with the time of exposure. The thickness of the threads has been tabulated against the exposure in Table 4.1.

No of Obs	Time of Exposure (sec) [TOE]	Energy (mJ/cm^2) [E=I*TOE]	lnE (mJ/cm^2)	Thickness of the cure thread (μm) [Cd]
1	60	372.6	5.920	470.25
2	90	558.9	6.326	515.54
3	105	652.05	6.480	542.22
4	120	745.2	6.614	572.76

Table 4.1: Thickness of the cure thread vs exposure time for in-house resin

The plot of cure depth versus the natural logarithm of Exposure ($C_d$vs lnE) has been shown in Fig 4.9. The slope of the plot is the depth of penetration

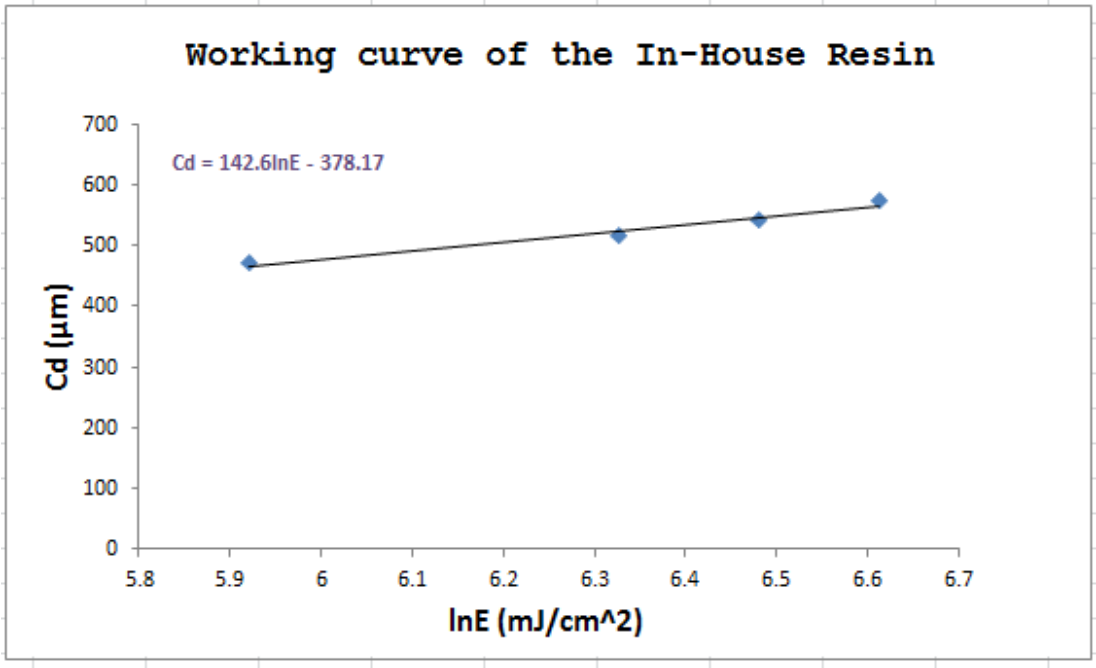

Figure 4.9: Working curve of the resin

while x-intercept of the plot is $ln(E_C)$ of the resin. Hence the D_p=142.6μm and E_c=14.18mJ/cm^2.

4.3.4.3 Commercial Resin

Spot-A materials company has also provided the E_c and D_p values for Spot-HT and Spot-E resin which are 10.35 mJ/cm and 122.94μm for Spot-HT while 11.55 mJ/cm and 143.25600μm for Spot-E resins. It is recommended in the literature that the values of E_c and D_p generally vary from the company values as the light source has been changed [16]. In order to verify these values the same experiment has been repeated for Spot-HT material.

The same experiment has been repeated for Spot-HT material and the working curve of the resin has been shown in Fig 4.10.

No of Obs	Time of Exposure (sec) [TOE]	Energy (mJ/cm^2) [E=I*TOE]	lnE (mJ/cm^2)	Thickness of the cure thread (μm) [Cd]
1	120	745.2	6.614	495.8
2	210	1304.1	7.173	560.68
3	240	1490.4	7.307	585.16
4	270	1676.7	7.425	593.8

Table 4.2: Thickness of the cured thread vs exposure time for Spot-HT resin

The E_c and D_p value of the Spot-HT resin is 13.33mJ/cm^2 and 123.1 μm. The E_c value is different from the company value and the possible reason for this is the light source whereas D_p value is almost same with the Spot-A company values.

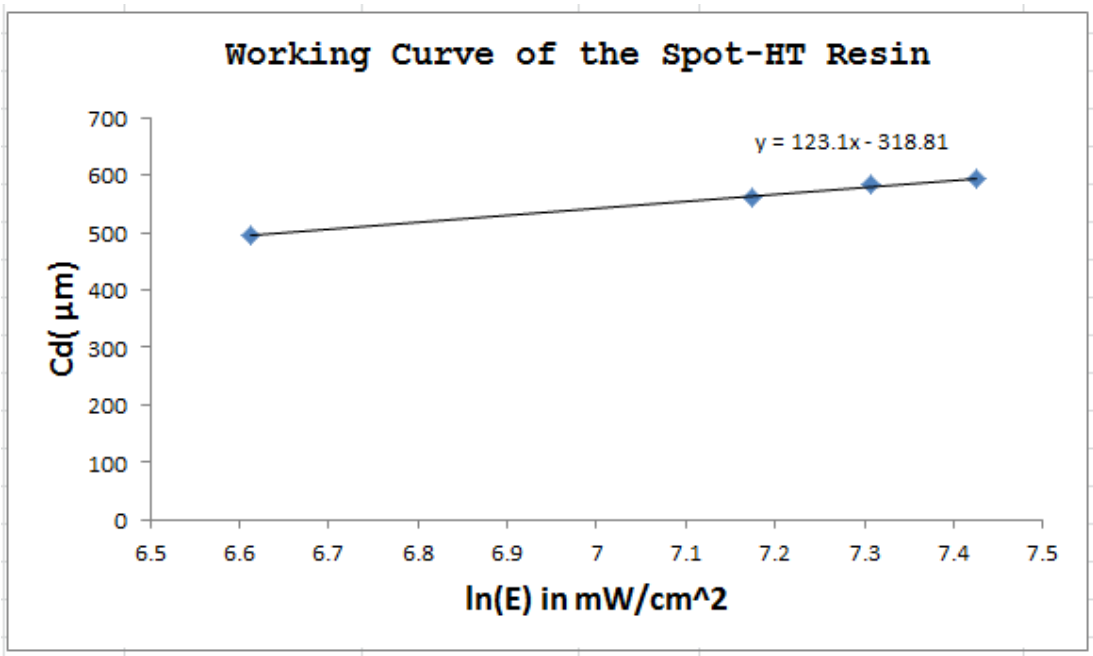

Figure 4.10: Working curve of Spot-HT resin

4.4 Cure Model

In order to cure dimensionally accurate parts the time of exposure required to cure single layer need to be find. The calculation of exposure time depends upon the layer thickness, no of layers and desired hight of the part. The platform move down 0.0664725mm in 60 seconds when the layer thickness is $0.01\mu m$.

$$TOE = 60 * [H]/[0.0664725] \tag{4.9}$$

$$SL = TOE/LN \tag{4.10}$$

$$C_d = D_p * ln(I * SL/E_c) \tag{4.11}$$

where:
TOE = Total exposure time for whole production in seconds.
H = Desired hight of the cured part.
SL = Exposure time for single layer in seconds.
LN = Total no of layers.
C_d = cure depth.
D_p = Penetration Depth.
E_C = Critical Energy.

I = Irradiance of the DLP projector receiving at the surface of the platform.

The total production time and exposure time for single layer can be calculated using above equations. If the layer thickness will change than the distance that platform will travel will also change and Equation 3.9 will be modified accordingly. Also the matlab code has been written to calculate exposure time for single layer as well as for whole production in Appendix C2.

4.5 Softwares

4.5.1 Solidworks

Solidwork is a tool that is used to designed the desired part for fabrication purpose. As in image formulation model it has been found that 4.5118029 mm in solidwork = 1mm on the platform. Hence considering this relation the part has been designed and than saved as a STL format for slicing purposes.

4.5.2 Flash Point Software

For slicing the STL file into layer, flashpoint software has been utilized as shown in 4.11. The layer hight can be decided manually during the slicing process. The minimum layer hight is 0.001 mm and exposure time can be adjust according to the cure model value.

4.5.3 Matlab

Matlab has been used for programming the light intensity of LED spectrum and projected image size on the platform. The codes are attached in the Appendix C.

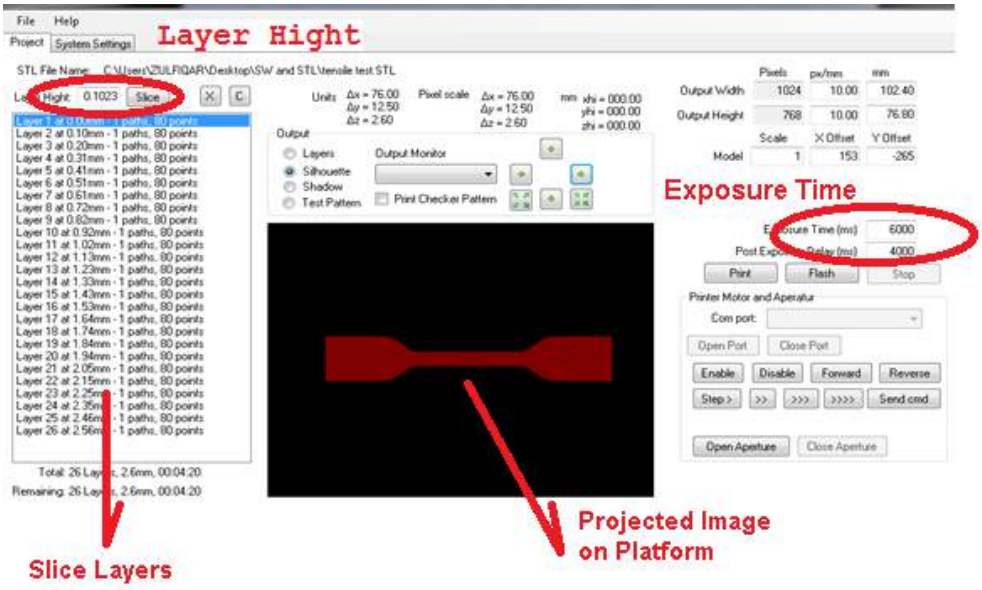

Figure 4.11: User interface of the slicing software

4.6 Summary

The summary of the process modeling has been shown in In Fig 4.12. In order to see that, the model is working accurately than there should be some case studies that need to be study which will verify the accuracy of the model. However, this model is limited toward the lateral direction dimension of the part hence high aspect ratio structures may be problematic for it.

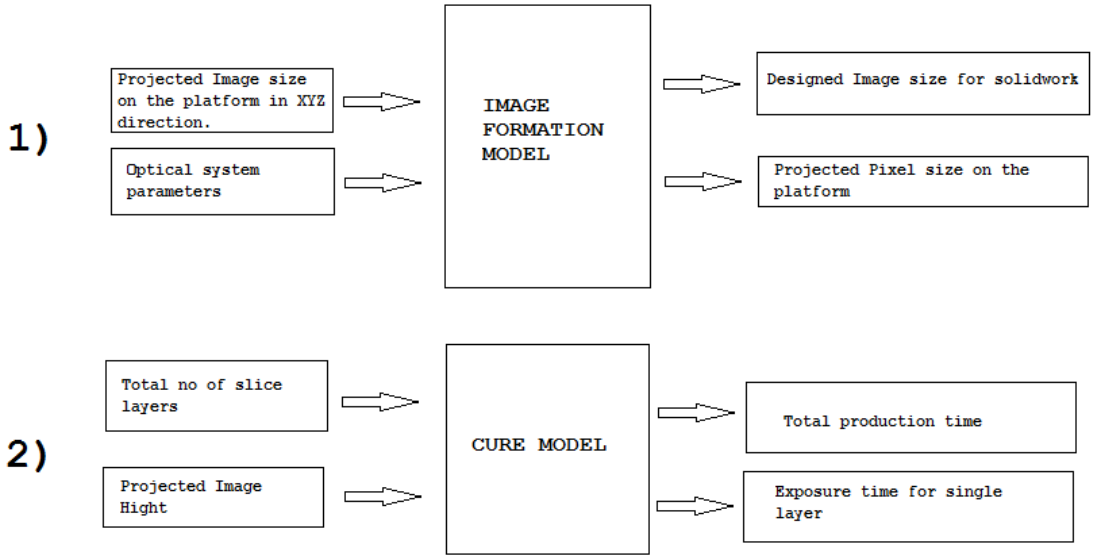

Figure 4.12: Block Diagram Projected Image and Cure Model

Chapter 5

Validation of Image Formulation and Cure Model

Different shapes based production has been done to ensure that the parts are built according to their intended designs.

5.1 Case Studies

5.1.1 Curing of a circle

A solid circle of diameter 10 mm in the lateral direction and thickness 1.5mm need to be cured via DLP based projection stereo lithography. The curing of this shape can be done by finding the design image size for CAD software in order to get 10mm on the platform via image formulation model. Than, convert the CAD file into STL format and slice it into desired no of layers via flashpoint slicing software. At the end, find the exposure time of a single layer using cure model.

From image formulation model it has been found that in order to get the image size of 10mm in the platform we need to design a circle of diameter 45.1180mm in terms of lateral dimensions and thickness of 6.7677mm in vertical dimensions.

The STL file of circle has been sliced into layers with layer hight 0.1mm. The total no of layers that has been made from flashpoint software is 68 with layer height 0.1mm. Now using cure model the exposure time of single layer has been found which is 20 seconds and total production time is 23 minutes. Optical microscope has been used to measure the diameter of the cured circle.

The diameter comparisons of the designed circle vs cured circle has been shown

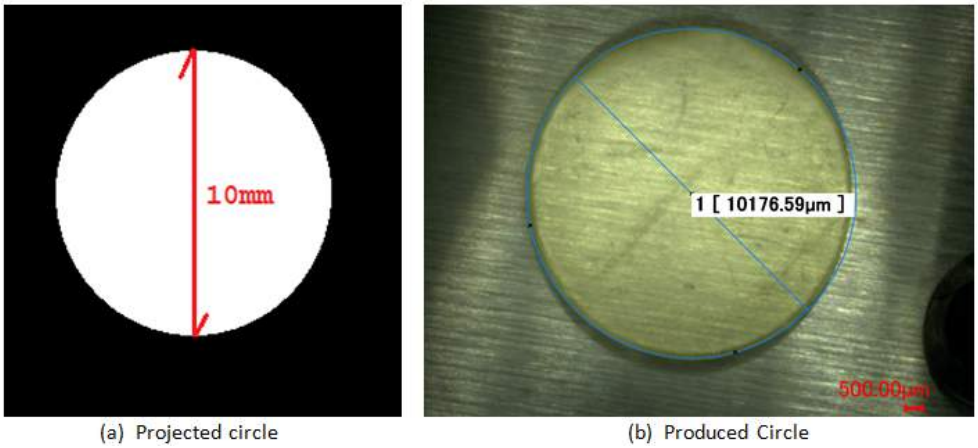

Figure 5.1: Projected circle vs cured circle.

in Fig 5.1. The diameter of the cured circle is 10.177mm which is very close to the projected image size. The percentage error in the diameter of the cured and design circle is 1.77% where positive sign shows that the produced part is bigger than the design part.

5.1.2 Curing of a square

A solid square of length 5 mm in the lateral direction and thickness 1.0 mm need to be cured via DLP based projection stereo lithography.

In a similar way all the steps has been followed and using Image formulation model and it has been found that a square of size 22.5590mm in the lateral direction and 4.5118mm in vertical direction need to be designed in solidwork software. The no of layers that are made after slicing the STL file are 46 with layer height 0.1mm. Using cure model the exposure time for single layer has been found which is 20 seconds and total production time is 15 minutes. The length of the cured square is 5.08mm where the projected image length is 5mm. The

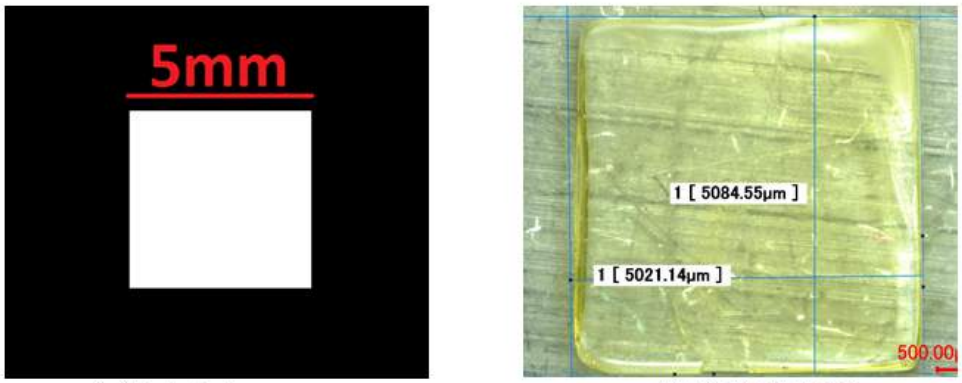

(a) Projected square (b) Produced square

Figure 5.2: Projected square vs cured square.

percentage error between cured square and designed square is 1.6%. However, the edges of the square are not as sharp as it was projected instead it is bit round. The possible reason for this error is the spherical aberration of the optical system.

5.1.3 Curing of a Hexagon Shape

The above shapes were solid and easy to cure. However, curing of a shape that have specific angles at the edges and holes will be a good example to verify the validity of image formulation and cure model. A hexagon shape has been choose to see this phenomena as it has both hole and angle at the edges. Fabrication of a hexagon shape with dimensions as shown in Table 5.1 and Fig 5.3 and the hight of the hexagon is 2 mm has been done to see the system limitation.

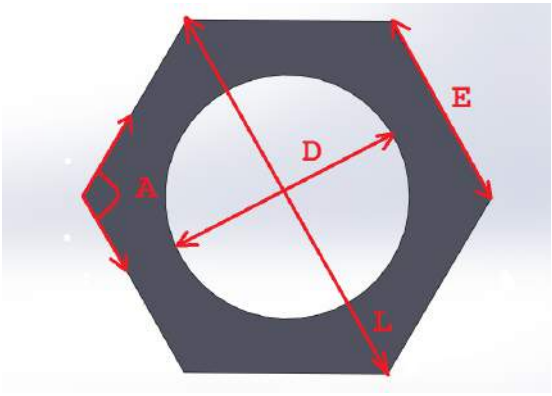

Figure 5.3: Projected image on platform

Using the Image formulation model the shape has been designed in the solid work and than using cure model the exposure time has been found which is 20 seconds for single layer where the total no of layers were 91. The whole production time is 30 minutes. After production finish the part was cleaned via isopropyl alcohol. Then using optical microscope the image has been taken which is shown in Fig 5.4. The dimenshion of the cured hexagon with the design hexagon has been shown in Fig 5.5.

Figure 5.4: Optical microscope image of Hexagon

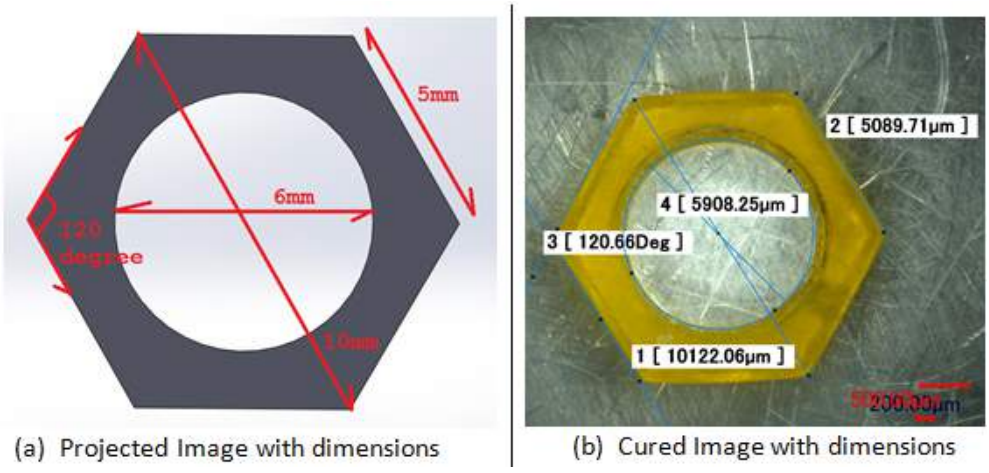

Figure 5.5: Projected vs Cured Hexagon

The comparison of the produced part with the design has been shown in Table 5.1. The percentage error in each direction has been calculated in which the positive sign shows that the part has been produced bigger than the original size

Parameters	Projected Image (mm) PI	Cured Image (mm) CI	Percentage Error (PE in %) PE = $\left(\frac{CI-PI}{PI}\right)$*100
L	10	10.122	1.22
E	5	5.089	1.78
D	6	5.908	-1.53
A	120	120.66	0.55

Table 5.1: Dimension comparisons of Designed and Cured Nut

while negative sign indicate opposite of it. The maximum error that has been found from this case study is 1.78%.

5.2 Error Correction Model

From the above case studies it has been found that the part has been produced via DLP based PSLA setup has an error in term of the lateral dimension. However, for fabricating accurate parts it is require to correct the errors. Therefor, the relation between projected image and fabricate image has been modeled which will lead towards accurate projection of the image.

5.2.1 Empirical Study

An empirical study has been done to find the relation between the projected and produce part. Different projection image size base experiments has been conducted as shown in Table 5.2. After performing the experiments optical microscope has been used to find the produced part size and the measurements has been repeated five times to get rid of measurement error. The results of the experiments has been shown in Fig 5.6. The relationship between projected and produced part can be deduced from Fig 5.6 as shown in Equation 5.1.

No Of Observation	Projected Image size in mm (X)	Produced Part size in mm (Y)	No Of Observation	Projected Image size in mm (X)	Produced Part size in mm (Y)
1	2	2.0752	**11**	3.5	3.581
2	2.1	2.1294	**12**	4	4.0584
3	2.2	2.2452	**13**	6	6.065
4	2.3	2.338	**14**	6.1	6.1922
5	2.4	2.432	**15**	6.2	6.2588
6	2.5	2.5282	**16**	6.3	6.3746
7	3.1	3.141	**17**	6.4	6.4716
8	3.2	3.2722	**18**	6.5	6.5864
9	3.3	3.3774	**19**	8	8.1468
10	3.4	3.44	**20**	10	10.2014

Table 5.2: Projected vs Produced image size experiments

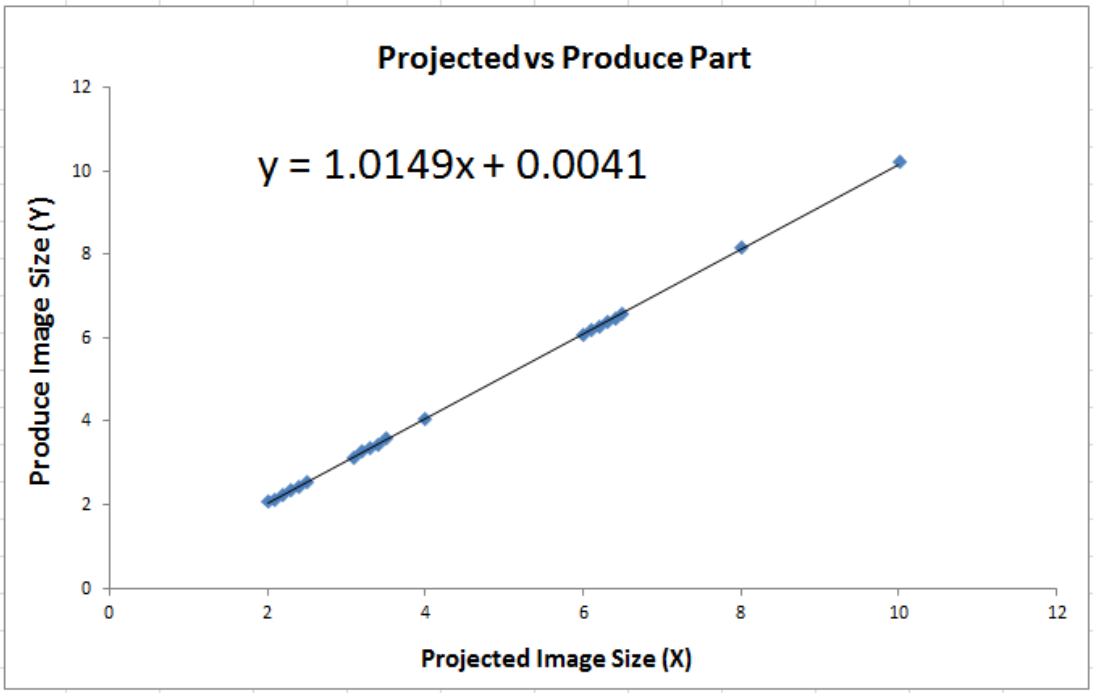

Figure 5.6: Error Correction Model

Using this relation it can be find that what is the projected image size need to be projected on the platform in order to get the desired dimension in the produced part.

$$ProjectedImagesize(X) = 0.9853[ProduceImagesize(Y)] - 0.0040 \qquad (5.1)$$

In order to test the model either it is working or not a sample production has been done. Firstly, 4 mm size base square has been projected on the platform and it has been produced via the DLP setup. The size of the produced part has been measured via optical microscope which is 4.106 mm as shown in Fig 5.7(a). The % error that has been found between produced part and projected part is -2.65% where negative sign indicate that produce part is larger than the project image. For correcting this error the above model has been used and it has been

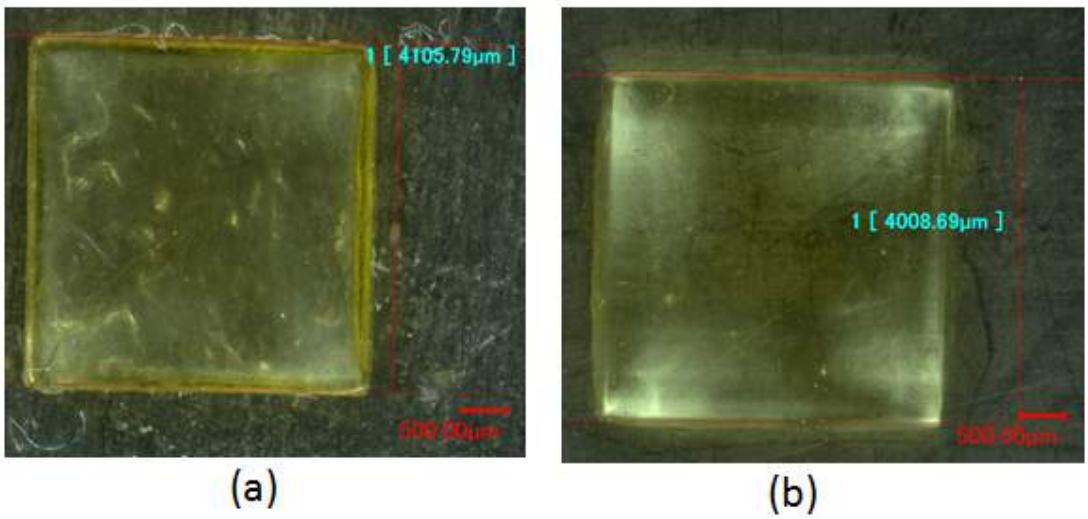

Figure 5.7: (a) Projected Image Size is 4mm , (b) Projected Image size is 3.94mm

found that in order to get 4 mm at the end of the production we need to project 3.94 mm image size. The production has been done using the projected image size 3.94 mm and the optical measurement of the produce part has been shown in Fig 5.7(b). The produced image size is 4.009 mm. The % error in this case is reduce to -0.225 %. This example shows that the error has been correct via error correction model and the produce part is more closed to original dimension that has been projected at the beginning.

5.2.2 Comments on Case Studies

From the results of above case studies, it can be concluded that the maximum percentage error in the lateral direction of the part is no more than 2%. These errors indicate that lateral dimension of the produced part can be control via image formulation and cure model and the part will be cure in 2% error in lateral direction. However, using error correction model these error can be controlled via projecting proper image size on the platform. Also, during the case study of square and hexagon shape the final part that has been cured is not as much sharp as it was sharp in the original design. The cured shape of the corner is bit round instead of sharp corners. The possible reason for this error is the misalignment between the optical lenses and DLP projector which causes the spherical aberration on the final image that is projecting on the platform.

5.3 Layerless Production using DLP PSLA setup

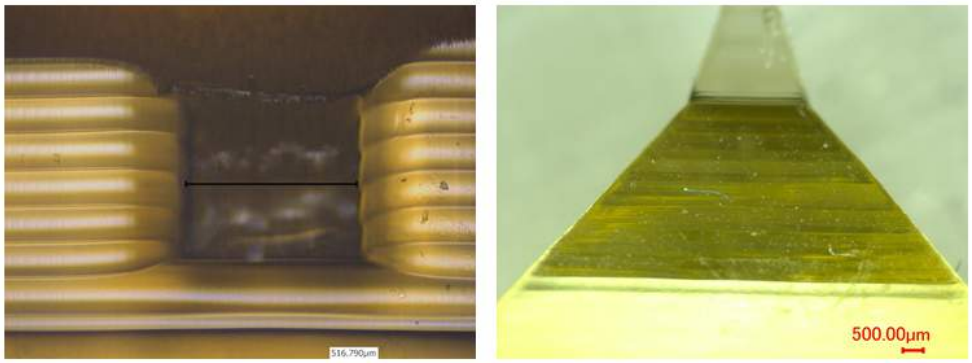

Figure 5.8: (a) Layer by Layer production, (b) Layerless production

The DLP based PSLA setup is a flexible setup that has capability of producing layer by layer (LBL) production as well as layerless (LL) production of a part as shown in Fig 5.8. Although, LL production have layers but its thickness is very small as compare to others. The continuous movement of the platform make the layer thickness small which ultimately seems like a layerless structure.

5.3.1 Surface Quality of the layerless (LL) production

The surface quality of the LL part will be better than the part that is made from LBL technique. A circular disc base production has been done to verify the

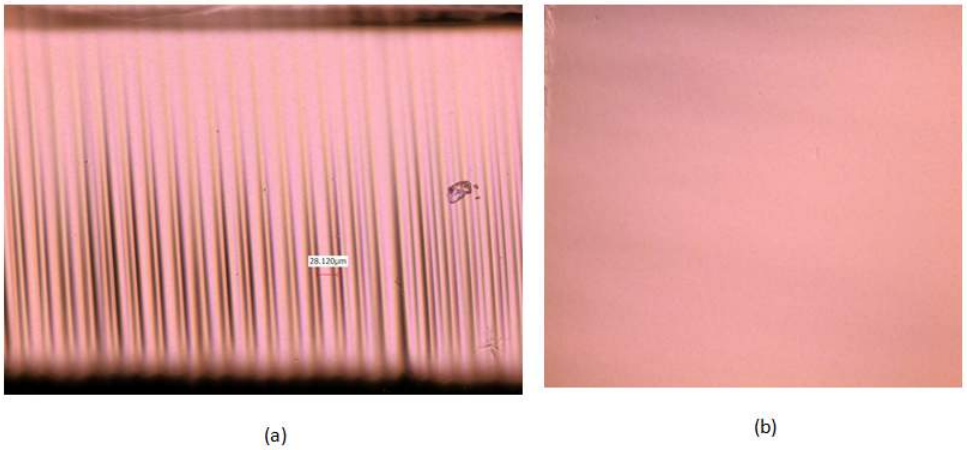

Figure 5.9: (a) Layer by Layer production with layer thickness $25\mu m$, (b) Layerless production

surface quality of both processes. A LBL production of a circular disc and LL production of a circular disc has been compared with respect to surface roughness and surface quality.

The laser microscope image has been captured for both production as shown in Fig 5.9. The layer thickness for LBL production is $28\mu m$. The surface profile that is achieved after the productions from both process has also shown in Fig 5.10. It can be seen from the surface profile that the surface roughness of LBL production will be more than the LL production. The surface roughness for LBL productions is 4.190 μm where as it is $0.285\mu m$ for LL production as shown in Fig 5.11. Hence, the surface roughness has decrease in case of LL production and the surface quality is improved. The LL based production has more smooth surface as compare to LBL production as shown in Fig 5.9.

Moreover, the system is capable of producing LBL and LL productions that is a new thing in the existing setups (except CLIP setup). The surface roughness of LL production can also improve more by reducing the layer thickness value.

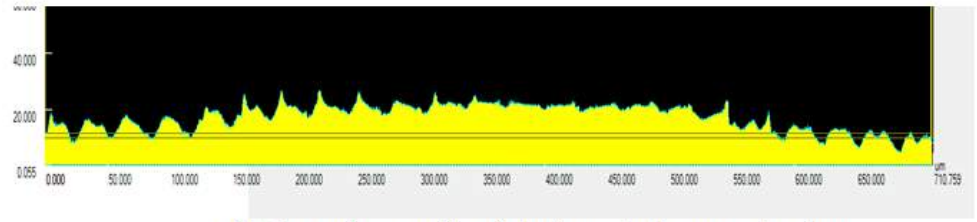

(a) The surface profile of the Layer by Layer production

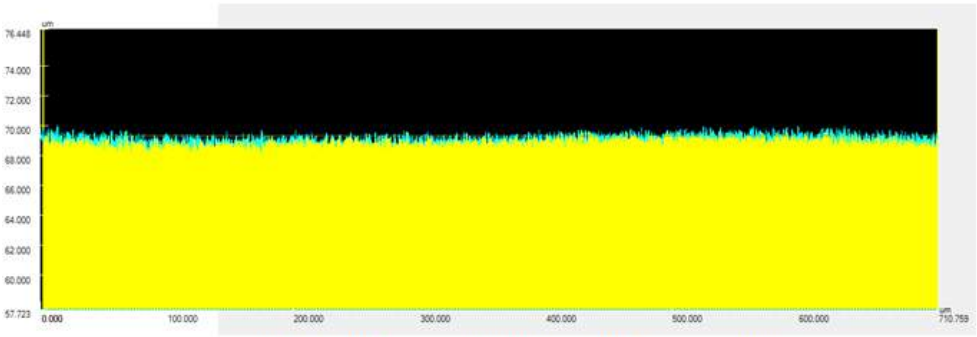

(b) The surface profile of the Layerless production

Figure 5.10: Surface Profile measurement for both productions.

	Rp	Rv	Rz	Ra
Total	12.849um	15.416um	28.265um	4.190um
Max.	12.849um	15.416um	28.265um	4.190um
Min.	12.849um	15.416um	28.265um	4.190um
Ave.	12.849um	15.416um	28.265um	4.190um
Std. DV	0.000um	0.000um	0.000um	0.000um
3sigma	0.000um	0.000um	0.000um	0.000um

(a) Surface roughness of Layer by Layer production

	Rp	Rv	Rz	Ra
Total	1.569um	1.643um	3.212um	0.285um
Max.	1.569um	1.643um	3.212um	0.285um
Min.	1.569um	1.643um	3.212um	0.285um
Ave.	1.569um	1.643um	3.212um	0.285um
Std. DV	0.000um	0.000um	0.000um	0.000um
3sigma	0.000um	0.000um	0.000um	0.000um

(b) Surface roughness of Layerless production

Figure 5.11: Surface roughness of both productions

5.4 Fabrication of 3D micro parts

5.4.1 Batch of Microneedle

Microneedle is a good example to know the capability of the setup to produce micro parts or not. A batch of 9 micro needle on a sequare has been designed accordingly as shown in Fig 5.12(a).

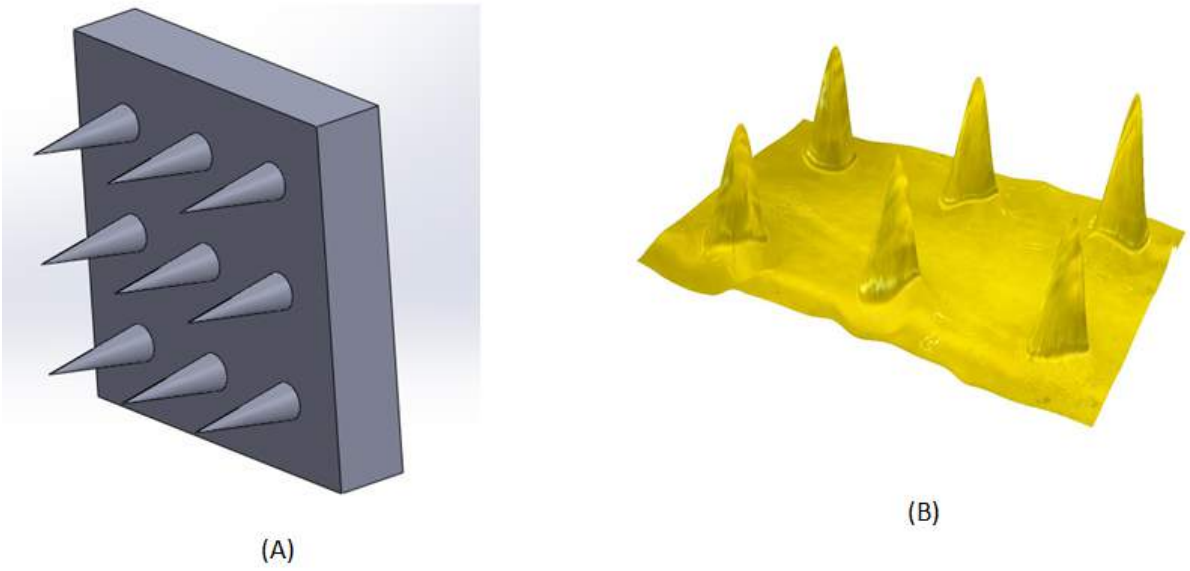

Figure 5.12: (A) Isometric view of the needle batch, (B) Optical microscope 3D view.

After applying the same image formulation and cure model the micro needle has been fabricated as shown in Fig 5.12(b). Also, the SEM images of the needles has been taken which verify the geometry of the needle as shown in Fig 5.13. In addition, a micro needle patch of base with Spot-E resin and the needle with the Spot-H resin has also been produced which make the micro needle patch flexible. The base of the micro needle patch can bend as it is made from Spot-E resin whereas the needle of the patch is made from Spot-H resin. However, the size of the tip of the needle is hard to maintain as during the cleaning process mostly the tip of the needle get damage. A careful cleaning can solve this problem but still the chances of the tip getting damage is high.

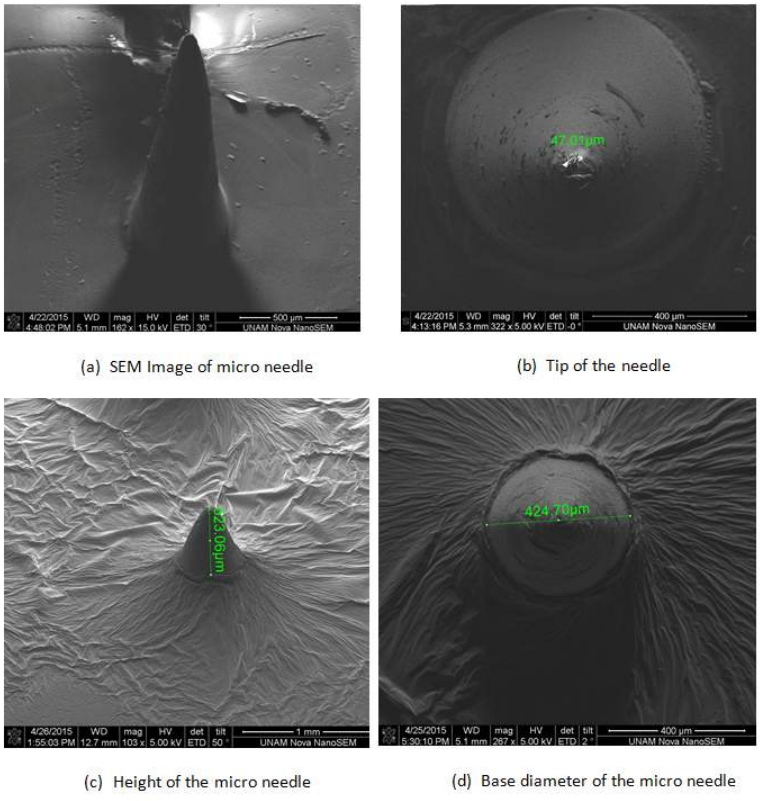

(a) SEM Image of micro needle

(b) Tip of the needle

(c) Height of the micro needle

(d) Base diameter of the micro needle

Figure 5.13: SEM images of the microneedle

5.5 Micro Hair and Variable Elasticity Structure

Different type of structure has been produce in order to see the capability of the setup. The micro hair based structure has been produced as shown in Fig 5.14. The diameter of a single thread in this micro hair structure is 120 μm.

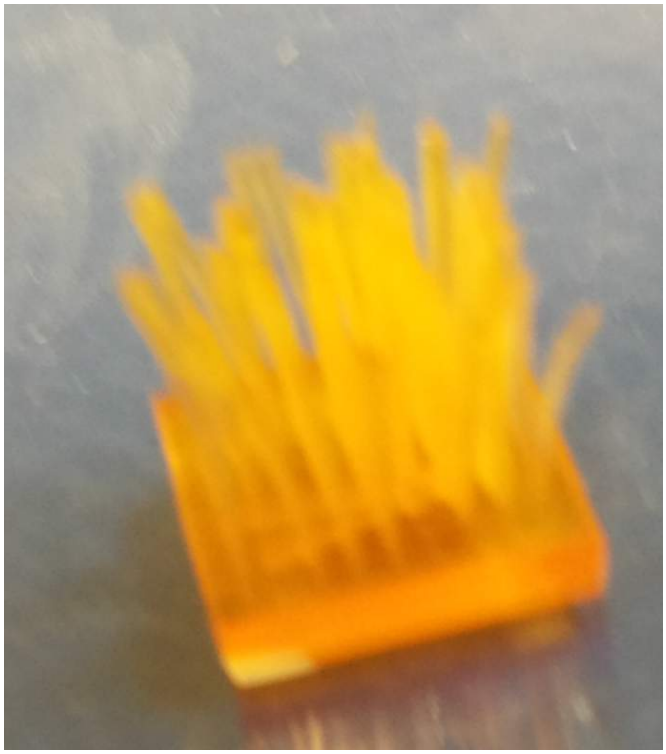

Figure 5.14: Microhair structure

A combination of both commercial and domestic resin has also been used to produce variable elastic structure as shown in Fig 5.15. Similarly Helical type structure has also been produced as shown in Fig 5.16. However, the helical structure has a bit overcure error which is discussed in section 5.5.

These production examples show that the setup can be used as a microstereolithography system too. Also, versatile production is possible by doing production carefully.

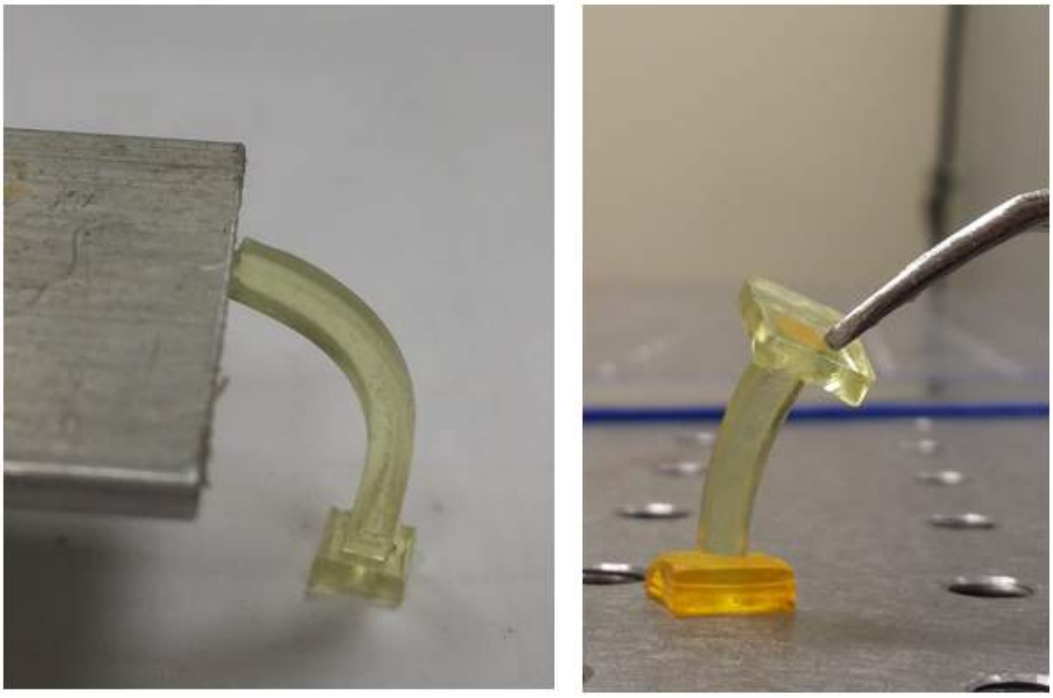

Figure 5.15: variable elasticity structure

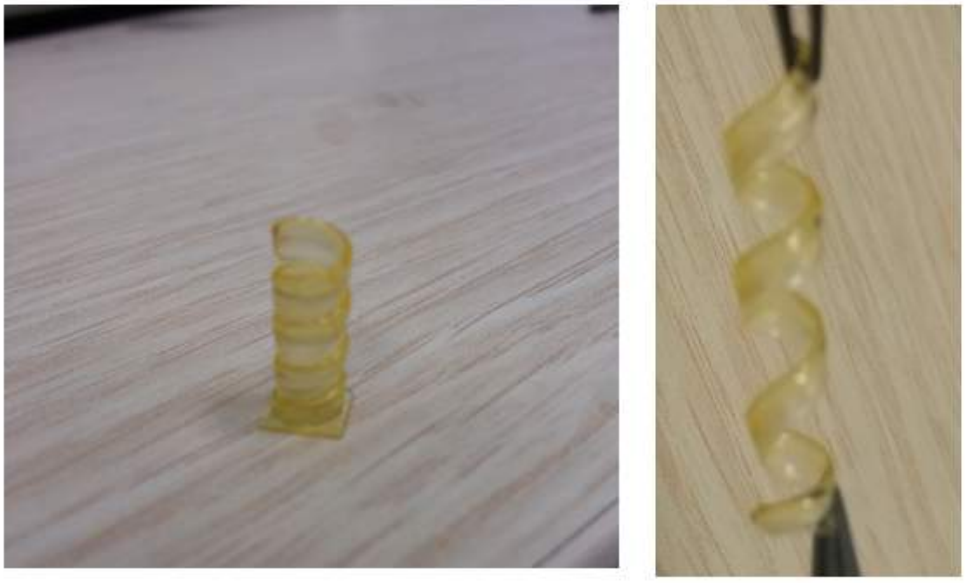

Figure 5.16: Helical Structure

5.6 Print through and over cure error

When a layer is cured using the DLP based PSLA system, its thickness is equal to the depth where the exposure falls to the threshold exposure E_c. The resin below this cured layer, though not receiving exposure equal to Ec, receives some exposure nevertheless. As more and more layers get cured, this point in the resin receives more and more exposure and finally, undergoes curing when the total exposure received by it equals or exceeds Ec. This results in unwanted curing and the error introduced is called as the print through error. The print through error can be seen in the above high aspect ratio structure as shown in Fig 5.17.

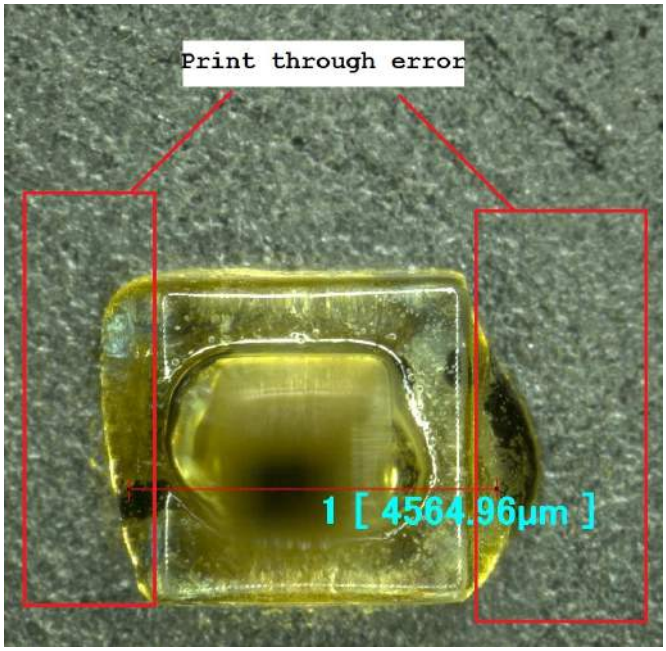

Figure 5.17: Print through error at light intensity 274mA.

Overcure error occurs when a single layer forms an overhang on any surface. The irradiation distribution across a typical square image formed by imaging a bitmap on the resin surface is such that the central part of the image gets over-exposed. As a result, the central portion of any layer will get cured to a depth larger than the intended layer thickness. The resulting error in the Z dimension of the micropart is referred to as the overcure error. If we want to manufacture dimensionally accurate 3D parts, there errors will have to be minimized. Just like in conventional Stereolithography, the print through errors can be minimized by

a method called Layer compensation, where a few bottom layers are deliberately skipped to compensate for the unwanted curing that occurs due to print through. Overcure errors can be eliminated by decreasing the time for which the bitmap is imaged onto the resin surface.

5.7 Resolution of the setup

There are two different resolutions on a DLP based PSLA apparatus: lateral resolution, and vertical resolution. Lateral resolution: is decided by the size of the individual mirror on the DMD as well as the focusing lens system. Vertical resolution: is simply determined by the layer thickness; the smaller the layer thickness, the better the vertical resolution. The theoretical value of the lateral resolution should be $23.276\mu m$ according to the image formulation model. An experiment has also been performed to verify this theoretical value in which a square shape part has been designed and fabricated using PSLA system. The pixel size has been measured after curing the part as show in Fig 5.18. The

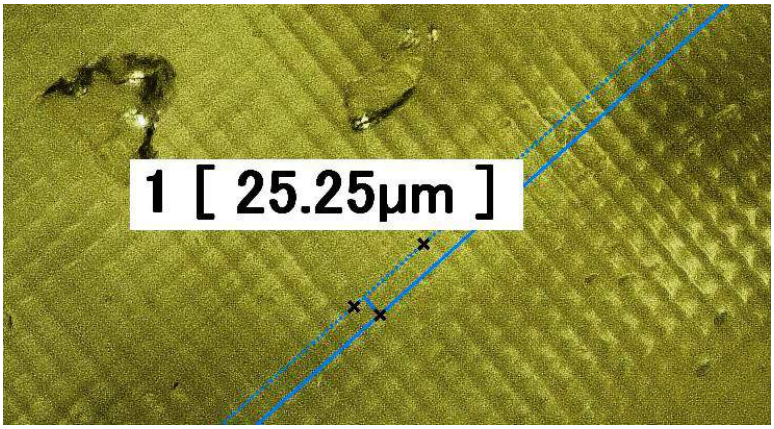

Figure 5.18: Pixel size after curing the part.

theoretical value of the projected pixel is $23.276\mu m$ where the measured value is $25.25\mu m$ which is approximately match with the model value. Hence, the lateral resolution of the system that has been find from the experiment is $25.25\mu m$. The maximum area that we can cure using this setup is 11.1726mm in x-direction and 14.8968mm in y direction. However, the platform has clear image at the

18.6174mm hight and it can go down to -30mm down hence the maximum hight that can be possible with this setup is 48.6174mm.

5.8 Summary

Different case studies has been conducted in order to show the validity of the image formation and cure model. Also, different structures has been fabricated to see the flexibility of the system. The lateral resolution of the setup has been find experimentally which is $25.25\mu m$. The comparisons of build PSLA setup with others printers has been shown in Table 5.3.

PμSLA Printers	**Sun.et PμSLA**	**Hadiposespito PμSLA**	**Limaye PμSLA**	**Pekka Lehtinen PμSLA**	**Bilkent DLP PSLA**
UV light Source	Mercury lamp	Mercury lamp	Mercury lamp	Video Projector	DLP Projector
Type of Translation Stage(TS)	Motorized	PC-controlled three axis micro-stage	Translation Translation	Stepper Motor System	Nano-positioning system
Resolution of the (TS)	0.1 μm	30 nm	N/A	5μm	2nm
Type of Production	Layer by layer Production	Layer by layer Production	Layer by layer Production	Layer by layer Production	layer by laery and layerless production
Fabrication Approach	Top to down movement of the platform	Top to down movement of the platform	Top to down movement of the platform	Bottom to up movement of the platform	top to down movement of the platform
Lateral Resolution	N/A	20μm	20μm	N/A	25.25μm
Chemical Resin	Commercial	Commercial	commercial	commercial	commercial, domestic
Main contribution	Development of PμSLA setup and its process modling	Improve the existing setup of PμSLA and did resin characterization	Development of PμSLA setup model its process and resin characterization	PμSLA setup was build and computer programming to run it.	Development of DLP based PSLA Setup and model its process and resin characterization

Table 5.3: Comparisons of the PμSLA setups with Bilkent DLP setup

Chapter 6

Conclusion and Future Work

In this thesis, a DLP based PSLA setup had been established successfully. The setup is constructed using commercially available and self-made components aiming at a minimum cost, which would ease the spreading of PSLA technology to other research groups in the future. As a part of this thesis, this setup has been established and different productions and trials has been done in order to verify the functionality of this printer. The established setup has a lateral resolution 25.25 μm and different complex shape can be fabricated easily. The main advantage of this setup is that it have a capability to produce layerless production which effect the surface quality of the part. All the setups that has been discussed in the literature review do not have this feature. Also, high aspect ratio structures can be fabricated through system by playing with the system parameters.

Moreover, the image formation and cure model has been modeled in order to predict the projected size of the part. The % error of these model in lateral direction is 2% which is quite good. From the results of different case studies, it has been seen that the part is fabricated within the 2% error range. The setup is quite flexible and different resin can be used on it e.g. commercial and domestic resins has been used for curing purposes. Composite polymer structures has also been achieved via this system with good surface quality. Similarly production of micro parts can be done with it e.g. microneedle patch has been created through this setup with tip diameter $48\mu m$.

6.1 Scope and Limitation

This research had the objective of formulating a process planning method for DLP based PSLA. The system that has been developed is a very simple embodiment of the stereo lithography principle. The process planning method has been developed for the layerless curing process using this system. This method can be leveraged across to most of the PSLA systems. In the Image formulation model, the alignment of all the components of the system is assumed to be perfect. Since the system is assembled manually, we expect some misalignments in the system. The effects of these misalignments have not been captured by the analytical model. As a result, there is still some discrepancy in the layer dimensions computed by the Image formulation model and the dimensions of the layer actually cured using the system. Also, the sharp corners error in the case study is probably due to misalignment in the system.

One of the limitation of the model is that if the light intensity and speed of the projector is remain same throughout the curing than for high aspect ratio structures undercuring/overcuring problem can be face which ultimately increase the % error in the dimensions.

6.2 Future Work

Experiment with DLP Projector: The DLP projector is a very flexible device. The light engine that has been attached in it can be disassembled and instead of broadband LED as a light source a UV LED can be assembled with it. Also, the system control of DLP projector is quite flexible and one can write his own program to use it accordingly.

Modify the Optical Systen: Optics of the system is the main area which provides the desired amount of resolution for the system. Higher resolution enables the user to produce smaller bases which increases the aspect ratio. In terms of developments, instead of using a single converging lens, it is possible to use a

system of lenses to provide high quality image with less optical aberrations. It is also possible to use a microscope lens array for better results [28].

Theoretical Model for vertical resolution: The vertical resolution is mainly depend upon the platform movement during the production. The vertical dimension is generally high as compare to the designed dimension and the main reason for this error is the position of the platform at the beginning time. As the platform is usually dip a bit high in the resin rather than the layer thickness which create this error. In addition, beginning position of the platform is not the same for every time . Hence there is a need of a theoretical model which can predict the error and able to improve it.

Chemical resin composition: Chemical mixture of the resin used is another area which has space for improvement. With different amount of Sudan-I mixture has also been tried during this study. The concentration of Sudan-I were like this (0.005,0.01, 0.015, 0.02 and 0.03) grams. One of the significant change that has been observed while using these resins is the time of exposure require to cure the resin start increasing as the Sudan-I concentration has increased in the resin. Further study can be done in order to see the mechanical properties of the produced parts from these resins.

Fabrication of Functionally graded Polymer: Functionally graded polymer are those polymers which have different property from one end of the part to other end and these properties change gradually as you move towards that end. As in chapter-5 it has shown that varied elastic polymers can be cured using DLP based PSLA setup than by doing some modification in the existing setup it is possible to cure functionally graded polymer.

Bibliography

[1] a. B. I.Gibson, D.W.Rosen, "Additive manufacturing technologies," *Springer Publisher,Book*, vol. 76, no. 12, pp. 1340 – 1344, 2010.

[2] S. Junk, J. Samann-Sun, and M. Niederhofer, "Application of 3D printing for the rapid tooling of thermoforming moulds," pp. 3–6. http://link.springer.com/chapter/10.1007%2F978-1-84996-432-6_83.

[3] C. K. Chua, K. F. Leong, and C. S. Lim, "Rapid prototyping principles and applications," 2010. http://www.worldscientific.com/doi/pdf/10.1142/9789812778994_fmatter.

[4] B. Khoshnevis, "Automated construction by contour crafting-related robotics and information technologies," *Automation in Construction*, vol. 13, no. 1, pp. 5–19, 2004.

[5] K.Moskvitch, "Printer produces personalised 3d chocolate," 2011. http://www.bbc.com/news/technology-14030720.

[6] P. Lehtinen, "Projection microstereolithography equipment," *aalto university school of science*, 2013.

[7] D. L. Victor, P. S. L. Gregory, and M. S. Steve, "Options for additive rapid prototyping methods (3d printing) in mems technology," *Rapid Prototyping Journal*, vol. 20, no. 5, 2014.

[8] E. Edge, "Stereolithography rapid prototyping review," http://www.engineersedge.com/sla_rapid_proto.htm.

[9] P.F.Jacobs, "Fundamentals of stereolithography," *3D Systems, Inc. Valencia, California*, 1992.

[10] X. X.Zhang and C.Sun, "Micro-stereolithography of polymeric and ceramic microstructures," *Sensors and Actuators*, vol. 77, pp. 149–156, 1999.

[11] K. H. Koji Ikuta, "Real three dimensional micro fabrication using stereo lithograpy and metal molding," pp. 42–47, 1992. http://ieeexplore.ieee.org/xpls/abs_all.jsp arnumber=296949 tag=1.

[12] B. K. Moskvitch, "Artificial blood vessels created on a 3d printer," 2011. http://www.bbc.co.uk/news/technology-14946808.

[13] D. X. C.Sun, N.Fang, "Projection micro-stereolithography using digital micro-mirror dynamic mask," *Sensors and Actuators*, vol. 121, pp. 105–111, 2005.

[14] X. Hadipoespito, G. W.; Li, "Microstereolithography based on digital micromirror device for complex meso/micro structures," *Transactions of NAMRI/SME*, vol. 121, pp. 113–120, 2005.

[15] J. R. Zyzalo, "Masked projection stereolithography:improvement of the limaye model for curing single layer medium sized parts," *PhD Thesis at massey univesity,albany,New Zealand*, 2008.

[16] D. A.S.Limaye, "Process planning method for mask projection microstereolithography," *Rapid Prototyping Journal*, vol. 13, no. 2, pp. 76–84, 2007.

[17] J. R. Tumbleston, D. Shirvanyants, N. Ermoshkin, R. Janusziewicz, A. R. Johnson, D. Kelly, K. Chen, R. Pinschmidt, J. P. Rolland, A. Ermoshkin, E. T. Samulski, and J. M. DeSimone, "Continuous liquid interface production of 3d objects," *Science Magazine Journal*, vol. 347, no. 6228, pp. 1349–1352, 2015.

[18] R. S. J. S. M. Hatzenbichler, M. Geppertb, "Additive manufacturing of photopolymers using the texas instruments dlp lightcrafter," *Emerging Digital Micromirror Device Based Systems and Applications V, edited by Michael R. Douglass, Patrick I. Oden,Proc. of SPIE*, vol. 8618, 2013.

[19] T. Instruments, "Dlp light crafter," 2013. http://www.ti.com/tool/DLPLIGHTCRAFTER.

[20] E. Company, "Aspheric and achromatic lens," 2013. http://www.edmundoptics.com/optics/optical-lenses/aspheric-lenses/aspherized-achromatic-lenses/2953/.

[21] K. Chockalingam, N. Jawahar, and U. Chandrasekhar, "Influence of layer thickness on mechanical properties in stereolithographye," *Rapid Prototyping Journal*, vol. 12, no. 2, pp. 106–113, 2006.

[22] F. point Slicing Software, "Flaspoint slicing software for stl file," http://sedgwick3d.com/FlashPoint/.

[23] Z. Y. C. Zhou, Y. Chen and B. Khoshnevis, "Development of a multi-material mask-image-projection-based stereolithography for the fabrication of digital materials," *Annual Solid Freeform Fabrication Symposium, Austin*, pp. 65–80, 2008.

[24] T. Instruments, "Dlp lightcrafter evaluation module (evm) users guide," 2013. http://www.ti.com/tool/DLPLIGHTCRAFTER.

[25] J.-P. Fouassier, "Photoinitiation, photopolymerization, and photocuring: Fundamentals and applications," 1995. http://www.amazon.com/Photoinitiation-Photopolymerization-Photocuring-Fundamentals-Applications/dp/1569901465.

[26] U. of illinois, "Establishment of stereolithography setup: (3d printing)," http://nano-cemms.illinois.edu/.

[27] professor nicholas fang, "Nanophotonics and 3d nanomanufacturing laboratory," http://web.mit.edu/nanophotonics/.

[28] P. Preechaburana and D. Filippini, "Snapshot mask-less fabrication of embedded monolithic su-8 microstructures with arbitrary topologies," *Procedia Chemistry.Proceedings of the Eurosensors XXIII conference*, vol. 1, pp. 778–781, 2009.

Appendix A

Digital Light Processing

A.1 DLP LightCrafter's Dimensions

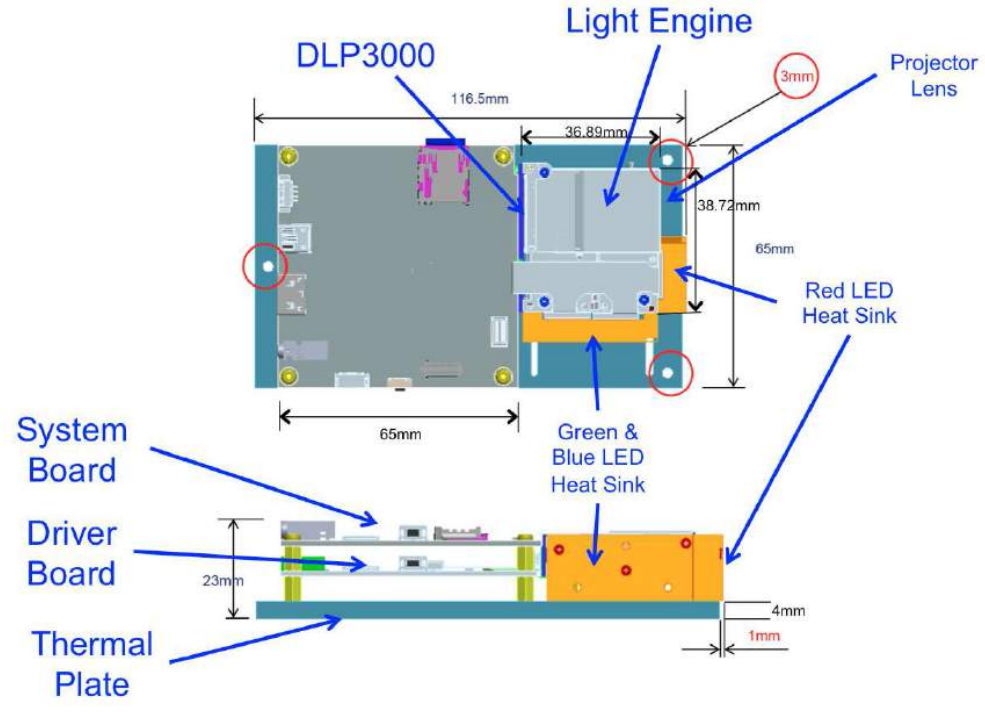

Figure A.1: DLP LightCrafter Module Dimensions

A.1.0.1 What is in the LightCrafter EVM?

The DLP LightCrafter module consists of three subsystems

- Light engine includes the optics, red, green, and blue LEDs, and the 608 x 684 diamond pixel 0.3-inch WVGA DMD. Capable of 20 lumens out-of-the-box with support to 50 lumens with users addition of active cooling.
- Driver board includes the LED driver circuits, DLPC300 DMD Controller, power management circuits, and MSP430.
- System board includes TMS320DM365, FPGA, and several connectors for external inputs.

A.1.0.1.1 Light Engine Young Optics, Inc. developed the DLP LightCrafters light engine as shown in Fig 3.2. The light engine consists of the following components:

- 0.3-inch WVGA DMD (DLP3000)
- OSRAM Red LED (LE A Q9WN)
- OSRAM Green LED (L CG H9RN)
- OSRAM Blue LED (LE B Q9WN)
- Murata NTC Thermistor (NCP15WF104F03RC)
- Optics with 1.66 Throw Ratio

Appendix B

Experiment Data Sheet

No of Obs	Speed	Light Intensity	Production Time in (min)	Obtained Width (w) in mm	original width (W) in mm	(W-w)	% error in Width	volume measured by Laser microscope in (mm)^3	Original Volume in (mm)^3	(original - measured) volume in (mm)^3	% error in volume
1	5	1	245	0.602	1	0.398	39.8	0.23424	0.5	0.26576	53.152
2	5	137	245	0.713	1	0.287	28.7	0.33515	0.5	0.16485	32.97
3	5	274	245	0.626	1	0.374	37.4	0.35168	0.5	0.14832	29.664
4	15	1	82	0.587	1	0.413	41.3	0.12284	0.5	0.37716	75.432
5	15	137	82	0.628	1	0.372	37.2	0.21612	0.5	0.28388	56.776
6	15	274	82	0.764	1	0.236	23.6	0.33688	0.5	0.16312	32.624
7	30	1	41	0.53	1	0.47	47	0.22807	0.5	0.27193	54.386
8	30	137	41	0.618	1	0.382	38.2	0.3209	0.5	0.1791	35.82
9	30	274	41	0.769	1	0.231	23.1	0.27853	0.5	0.22147	44.294

NOTE	
% error value Positive	The width/hight is smaller than the original
% error value Negative	The width/hight is bigger than the original

Figure B.1: Data Sheet of first Design of Experiment.

B.1 Two Way ANOVA Test Results

	No of Obs	Speed	Light Intensity	Production Time in (min)	Obtained Width (w) in mm	original width (W) in mm	(W-w)	% error in Width	Average Flatness error (in micron)	Average Flatness error (in mm)	% error in Flatness	volume measured by Laser microscope in (mm)^3	Original Volume in (mm)^3	(original - measured) volume in (mm)^3	% error in volume
Spheric Lens	1	6	1	203	0.733	1	0.267	26.7	17.11	0.01711	1.711	0.255	0.5	0.245	49
Spheric Lens	2	6	137	203	0.823	1	0.177	17.7	11.09	0.01109	1.109	0.31	0.5	0.19	38
Spheric Lens	3	6	274	203	0.837	1	0.163	16.3	12.3	0.0123	1.23	0.32	0.5	0.18	36
Spheric Lens	4	8	1	153	0.722	1	0.278	27.8	9.99	0.00999	0.999	0.25	0.5	0.25	50
Spheric Lens	5	8	137	153	0.774	1	0.226	22.6	10.59	0.01059	1.059	0.31	0.5	0.19	38
Spheric Lens	6	8	274	153	0.855	1	0.145	14.5	7.41	0.00741	0.741	0.42	0.5	0.08	16
Spheric Lens	7	10	1	123	0.699	1	0.301	30.1	10.16	0.01016	1.016	0.25	0.5	0.25	50
Spheric Lens	8	10	137	123	0.781	1	0.219	21.9	9.51	0.00951	0.951	0.3	0.5	0.2	40
Spheric Lens	9	10	274	123	0.841	1	0.159	15.9	8.73	0.00873	0.873	0.37	0.5	0.13	26
Spheric Lens	10	12	274	101	0.847	1	0.153	15.3	10.06	0.01006	1.006	0.35	0.5	0.15	30
Spheric Lens	11	8.5	274	143	0.837	1	0.163	16.3	10.1	0.0101	1.01	0.32	0.5	0.18	36
Spheric Lens	12	10.5	274	116	0.844	1	0.156	15.6	10.11	0.01011	1.011	0.34	0.5	0.16	32
Spheric Lens	13	9	274	135	0.802	1	0.198	19.8	7.63	0.00763	0.763	0.34	0.5	0.16	32
Achromatic lens	14	8	274	153	0.954	1	0.046	4.6	5.59	0.00559	0.559	0.45	0.5	0.05	10
Achromatic lens	15	6	274	203	0.93	1	0.07	7	8.23	0.00823	0.823	0.424	0.5	0.076	15.2

Figure B.2: Data Sheet of second Design of Experiment.

Two-way ANOVA: % Averge Error in Width vs Speed (nm/s), LI (mA)

Source	DF	SS	MS	F	P	
Speed (nm/s)	5	2008.72	401.744	92.30	0.000	(Significant)
LI (mA)	2	558.47	279.236	64.16	0.000	(Significant)
Error	10	43.52	4.352			
Total	17	2610.72				

S = 2.086 R-Sq = 98.33% R-Sq(adj) = 97.17%

Two-way ANOVA: % Average Error in volume vs Speed (nm/s), LI (mA)

Source	DF	SS	MS	F	P	
Speed (nm/s)	5	1813.21	362.642	7.90	0.003	(Significant)
LI (mA)	2	777.63	388.814	8.47	0.007	(Significant)
Error	10	459.10	45.910			
Total	17	3049.94				

S = 6.776 R-Sq = 84.95% R-Sq(adj) = 74.41%

Two-way ANOVA: % Average Error in Flatness vs Speed (nm/s), LI (mA)

Source	DF	SS	MS	F	P	
Speed (nm/s)	5	727.451	145.490	29.90	0.000	(Significant)
LI (mA)	2	22.676	11.338	2.33	0.048	(Significant)
Error	10	48.664	4.866			
Total	17	798.791				

S = 2.206 R-Sq = 93.91% R-Sq(adj) = 89.64%

Figure B.3: Results of Two-Way ANOVA using Minitab.

Appendix C

Code

C.1 Code to find the area under the curve and irradiance of each LED light spectrum.

Digitize data get from spectrum of the LED as shown in Fig4.4.

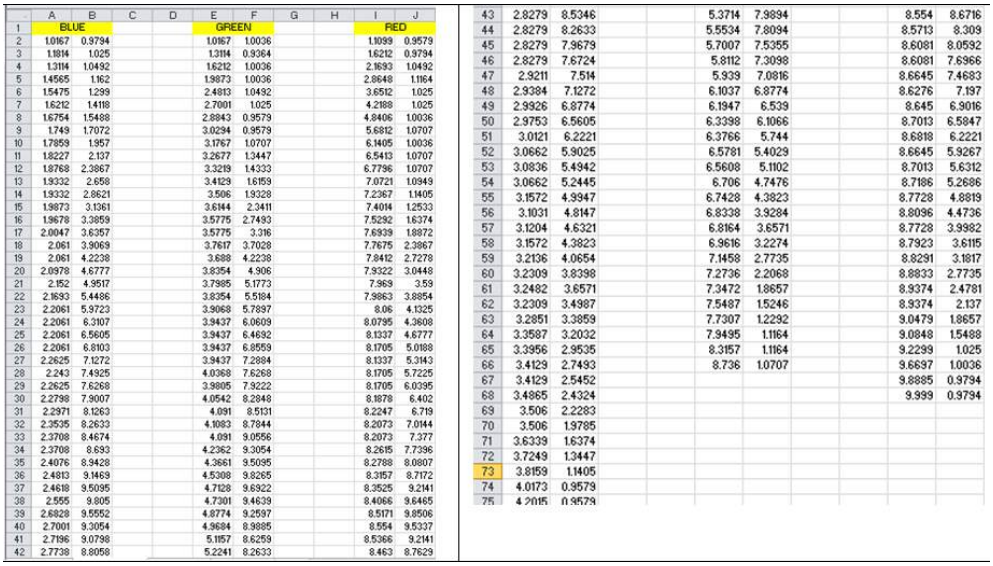

	A	B	C	D	E	F	G	H	I	J
1	BLUE				GREEN				RED	
2	1.0167	0.9794			1.0167	1.0036			1.1099	0.9579
3	1.1814	1.025			1.3114	0.9364			1.6212	0.9794
4	1.3114	1.0492			1.6212	1.0036			2.1693	1.0492
5	1.4565	1.162			1.9873	1.0036			2.8648	1.1164
6	1.5475	1.299			2.4813	1.0492			3.6512	1.025
7	1.6212	1.4118			2.7001	1.025			4.2188	1.025
8	1.6754	1.5488			2.8843	0.9579			4.8406	1.0036
9	1.749	1.7072			3.0294	0.9579			5.6812	1.0707
10	1.7859	1.957			3.1767	1.0707			6.1405	1.0036
11	1.8227	2.137			3.2677	1.3447			6.5413	1.0707
12	1.8768	2.3867			3.3219	1.4333			6.7796	1.0707
13	1.9332	2.658			3.4129	1.6159			7.0721	1.0949
14	1.9332	2.8621			3.506	1.9328			7.2367	1.1405
15	1.9873	3.1361			3.6144	2.3411			7.4014	1.2533
16	1.9678	3.3859			3.5775	2.7493			7.5292	1.6374
17	2.0047	3.6357			3.5775	3.316			7.6939	1.8972
18	2.061	3.9069			3.7617	3.7028			7.7675	2.3867
19	2.061	4.2238			3.688	4.2238			7.8412	2.7278
20	2.0978	4.6777			3.8354	4.906			7.9322	3.0448
21	2.152	4.9517			3.7985	5.1773			7.969	3.59
22	2.1693	5.4486			3.8354	5.5184			7.9863	3.8854
23	2.2061	5.9723			3.9068	5.7897			8.06	4.1325
24	2.2061	6.3107			3.9437	6.0609			8.0795	4.3608
25	2.2061	6.5605			3.9437	6.4692			8.1337	4.6777
26	2.2061	6.8103			3.9437	6.8559			8.1705	5.0188
27	2.2625	7.1272			3.9437	7.2884			8.1337	5.3143
28	2.243	7.4925			4.0368	7.6268			8.1705	5.7225
29	2.2625	7.6268			3.9865	7.9222			8.1705	6.0395
30	2.2798	7.9007			4.0542	8.2848			8.1878	6.402
31	2.2971	8.1263			4.091	8.5131			8.2247	6.719
32	2.3535	8.2633			4.1083	8.7844			8.2073	7.0144
33	2.3708	8.4674			4.091	9.0556			8.2073	7.377
34	2.3708	8.693			4.2362	9.3054			8.2615	7.7396
35	2.4076	8.9428			4.3661	9.5095			8.2788	8.0807
36	2.4813	9.1469			4.5308	9.8265			8.3157	8.7172
37	2.4618	9.5095			4.7128	9.8922			8.3525	9.2141
38	2.555	9.805			4.7301	9.4639			8.4066	9.6465
39	2.6828	9.5552			4.8774	9.2597			8.5171	9.8506
40	2.7001	9.3054			4.9684	8.9885			8.554	9.5337
41	2.7196	9.0798			5.1157	8.6259			8.5366	9.2141
42	2.7738	8.8058			5.2241	8.2633			8.463	8.7629
43	2.8279	8.5346			5.3714	7.9894			8.554	8.6716
44	2.8279	8.2633			5.5534	7.8094			8.5713	8.309
45	2.8279	7.9679			5.7007	7.5355			8.6081	8.0592
46	2.8279	7.6724			5.8112	7.3098			8.6081	7.6966
47	2.9211	7.514			5.939	7.0816			8.6645	7.4683
48	2.9384	7.1272			6.1037	6.8774			8.6276	7.197
49	2.9926	6.8774			6.1947	6.539			8.645	6.9016
50	2.9753	6.5605			6.3398	6.1066			8.7013	6.5847
51	3.0121	6.2221			6.3766	5.744			8.6818	6.2221
52	3.0662	5.9025			6.5781	5.4029			8.6645	5.9267
53	3.0836	5.4942			6.5608	5.1102			8.7013	5.6312
54	3.0662	5.2445			6.706	4.7476			8.7186	5.2686
55	3.1572	4.9947			6.7428	4.3823			8.7728	4.8819
56	3.1031	4.8147			6.8338	3.9284			8.8096	4.4736
57	3.1204	4.6321			6.8164	3.6571			8.7728	3.9982
58	3.1572	4.3823			6.9616	3.2274			8.7923	3.6115
59	3.2136	4.0654			7.1458	2.7735			8.8291	3.1817
60	3.2309	3.8398			7.2736	2.2068			8.8833	2.7735
61	3.2482	3.6571			7.3472	1.8657			8.9374	2.4781
62	3.2309	3.4987			7.5487	1.5246			8.9374	2.137
63	3.2851	3.3859			7.7307	1.2292			9.0479	1.8657
64	3.3587	3.2032			7.9495	1.1164			9.0848	1.5488
65	3.3956	2.9535			8.3157	1.1164			9.2299	1.025
66	3.4129	2.7493			8.736	1.0707			9.6697	1.0036
67	3.4129	2.5452							9.8885	0.9794
68	3.4865	2.4324							9.999	0.9794
69	3.506	2.2283								
70	3.506	1.9785								
71	3.6339	1.6374								
72	3.7249	1.3447								
73	3.8159	1.1405								
74	4.0173	0.9579								
75	4.2015	0.9579								

Figure C.1: Digitize data get from spectrum of the LED.

```
%%%%%%%%%%%%%%%%%%%%%%%%%%%%%%%%%%%%%%%%%%%%%%%%%%%%%%%%%%%%%%%%%%%%%%%%%%%%%%%%
%% Code to calculate the area under the curve and irradiance
of each LED light spectrum written by Zulfiqar Ali on 25 July 2015
%%%%%%%%%%%%%%%%%%%%%%%%%%%%%%%%%%%%%%%%%%%%%%%%%%%%%%%%%%%%%%%%%%%%%%%%%%%%%%%%
A=xlsread('LED2.xlsx','Sheet1','A2:A75'); % X-axis of Blue Light
(Wavelength in nm)
B=xlsread('LED2.xlsx','Sheet1','B2:B75'); % Y-axis of Blue Light
(Light Intensity)
E=xlsread('LED2.xlsx','Sheet1','E2:E66'); % X-axis of Green Light
(Wavelength in nm)
F=xlsread('LED2.xlsx','Sheet1','F2:F66'); % Y-axis of Green Light
(Light Intensity)
I=xlsread('LED2.xlsx','Sheet1','I2:I68'); % X-axis of Red Light
(Wavelength in nm)
J=xlsread('LED2.xlsx','Sheet1','J2:J68'); % Y-axis of Red Light
(Light Intensity)
plot(A,B,'color','b');hold on;
plot(E,F,'color','g');hold on;
plot(I,J,'color','r');
Blue_light_area = trapz(A,B)   % area under the blue light
Green_light_area= trapz(E,F)   % area under the green light
Red_light_area= trapz(I,J)     % area under the red light
b=Blue_light_area;
g=Green_light_area;
r=Red_light_area;
Total_Irradiance= 29.4602 %Irrdiance of a circle in mW/cm^2
of diameter 1.15cm
I=Total_Irradiance;
Total_bluelight_irradiance=(I*b)/(b+g+r)
Total_greenlight_irradiance=(I*g)/(b+g+r)
Total_redlight_irradiance=(I*r)/(b+g+r)
Ib=Total_bluelight_irradiance; %blue light irrdiance
using Ib=(I*b)/(b+g+r);
```

```
Ig=Total_greenlight_irradiance;%green light irrdiance
using Ig=(I*g)/(b+g+r);
Ir=Total_redlight_irradiance;%redlight irrdiance
using Ir=(I*r)/(b+g+r);
Total=Ib+Ig+Ir % Total iradiance=I_b+I_g+I_r
```

C.2 Image formoulation and cure model

```
%%%%%%%%%%%%%%%%%%%%%%%%%%%%%%%%%%%%%%%%%%%%%%%%%%%%%%%%%%%%%%%%%%%%%%%%%%%%%%%%
% Code to calculate the Pixel size of the Projected image on the
platform written by Zulfiqar Ali on 01-August-2015
%%%%%%%%%%%%%%%%%%%%%%%%%%%%%%%%%%%%%%%%%%%%%%%%%%%%%%%%%%%%%%%%%%%%%%%%%%%%%%%%

oy=input('The no of mirrors active vertically on the object = ');
ox=input('The no of mirrors active horizantally on the object = ');
Ho=oy*0.007637%Ho= no of mirrors active
vertically * size of the mirror (mm)
Wo=ox*0.007637% Wo= no of mirrors active
horizantally * size of the mirror (mm)
d_1=13.59;     % distance between DMD and Acromatic Lens in (mm)
d_2=41.42;     % distance between Acromatic Lens and platform in (mm)
M=d_2/d_1;     % Magnification formoula
Hi=Ho*M;       % Vertical size of Projected image (mm)
Wi=Wo*M;       % Horizantal size of the Projected image (mm)
Projected_image_Pixel_size_vertical=(Hi/oy)*1000
% Pixel size on the Projected image in um
Projected_image_Pixel_size_horizontal=(Wi/ox)*1000
% Pixel size on the projected image in um

%%%%%%%%%%%%%%%%%%%%%%%%%%%%%%%%%%%%%%%%%%%%%%%%%%%%%%%%%%%%%%%%%%%%%%%%%%%%%%%%
```

```
% Code to Calculate the Projected image size from flashpoint
to solidwork %
%%%%%%%%%%%%%%%%%%%%%%%%%%%%%%%%%%%%%%%%%%%%%%%%%%%%%%%%%%%%%%%%%%%%%%%%%%%%
x=input('The desired x-axis dimension on platform in mm = ');
% 1mm in flashpoint = 4.5118029411764705882352941176471mm in solidwork
y=input('The desired y-axis dimension on platform in mm = ');
z=input('The desired z-axis dimension on platform in mm = ');
x_dimension_in_solidworks=4.51180294117647058823529411764 71*x
% 1mm in solidwork = 0.221640885703054667724458658433 79 in flashpoint
y_dimension_in_solidworks=4.51180294117647058823529411764 71*y
z_dimension_in_solidworks=4.51180294117647058823529411764 71*z
hight=z;
%%%%%%%%%%%%%%%%%%%%%%%%%%%%%%%%%%%%%%%%%%%%%%%%%%%%%%%%%%%%%%%%%%%%%%%%%%%%
%%% What will exposure time require to cure single layer %%%
%%%%%%%%%%%%%%%%%%%%%%%%%%%%%%%%%%%%%%%%%%%%%%%%%%%%%%%%%%%%%%%%%%%%%%%%%%%%
LT=0.00001 % in mm
LN=input('Total no of slice layers = ')
Total_Exposure_Time_in_seconds=(60*hight)/0.0664725
% In 60 seconds platform will move 0.0664725 move down
TET=Total_Exposure_Time_in_seconds;
Total_Exposure_Time_in_minutes=Total_Exposure_Time_in_seconds/60
Total_Exposure_Time_in_hours=Total_Exposure_Time_in_minutes/60
ET_single_layer_in_seconds=TET/LN
ETSL=ET_single_layer_in_seconds;
ET_in_milliseconds=ETSL*1000

%%%%%%%%%%%%%%%%%%%%%%%%%%%%%%%%%%%%%%%%%%%%%
```